UNIVERSITY OF CRETE

FOUNDATION of RESEARCH AND TECHNOLOGY

Molecular Biology and Biomedicine (MBB) graduate Programme

Departments of Biology and Medicine

&

Instintute of Molecular Biology and Biotechnology (IMBB)

Laboratory of Developmental Neurobiology

Professor: Karagogeos Domna

Fakoureli Eirini

Master Thesis

"Investigating known and novel protein interactions of the cell adhesion molecule TAG-1 and its implication in the EAE mouse model"

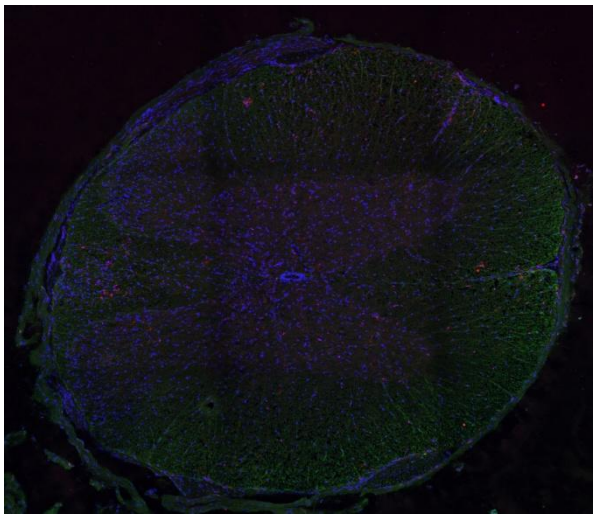

October 2016

TABLE OF CONTENTS

ABSTRACT

The main function of the myelin sheath is nerve insulation and subsequent increase of the speed at which electrical signals travel. The axo-glial interactions, which are the interactions between the glial cell and the adjacent axon, segregate the fiber in distinct molecular and functional domains that ensure the rapid propagation of action potentials. These domains are the node of Ranvier, the paranode, the juxtaparanode and the internode. They are characterized by multiprotein complexes between voltage-gated ion channels, cell adhesion molecules, members of the Neurexin family and cytosceletal proteins. TAG-1 (Transient Axonal Glycoprotein-1) a cell adhesion molecule of the Immunoglobulin superfamily, is expressed both by neurons and myelinating glia and is concentrated at the juxtaparanodes of adult central and peripheral nervous system. TAG-1 forms a tripartite complex with the Neurexin protein Caspr2 and the voltage gated potassium channels (VGKCs). More specifically, TAG-1 belongs to the Contactin subfamily which is characterized by four Fibronectin type III (FNIII) repeats and six Ig-like modules. Up to date, it has been shown that TAG-1 interacts in an homophilic way with itself *in trans* through its FNIII repeats. Moreover, it interacts in an heterophilic way *in cis* with Caspr2 and VGKCs through its Ig-like domains while FNIII repeats do not take place in this interaction. The study of these interactions is of high importance as the complete absence of either TAG-1 or Caspr2 results in disruption of the juxtaparanodal complex and subsequent diffusion of VGKCs towards the internode. In a variety of demyelinating pathologies including Multiple Sclerosis, the molecular architecture of the myelinated fiber is disrupted, leading to axonal degeneration.

In the first part of this study, we have analyzed the TAG-1 subdomains implicated in its interaction with Caspr2 and we investigated the role of a released form of TAG-1 in this interaction. Our results were contradictory with what was previously shown as almost all the TAG-1 subdomains, FNIII repeats included, could interact with Caspr2. Furthermore, we identified Semaphorin6A and Neurofascin isoforms 140 and 155 as novel interactors of TAG-1.

In the second part of this study, in an effort to further study the role of TAG-1 in myelination, we focused on the role of TAG-1 in the demyelination murine model of Experimental Autoimmune Encephalomyelitis (EAE). TAG-1 absence resulted in a delay in the development of neurological symptoms, linked to a reduced recruitment of regulatory T cells in the spinal cord.

ΠΕΡΙΛΗΨΗ

Η βασική λειτουργία του μυελώδους ελύτρου είναι η μόνωση των νευρικών κυττάρων και συνεπώς η αύξηση της ταχύτητας με την οποία μεταδίδονται τα ηλεκτρικά σήματα. Οι αξονο-γλοιακές αλληλεπιδράσεις, που είναι οι αλληλεπιδράσεις μεταξύ του γλοιακού κυττάρου και του παρακείμενου άξονα, διαχωρίζουν τα εμμύελα νευρικά κύτταρα σε διακριτές υποπεριοχές οι οποίες χαρακτηρίζονται από διαφορετική μοριακή οργάνωση και λειτουργία. Οι υποπεριοχές αυτές είναι ο κόμβος του Ranvier, η παρακομβική, η εγγύς της παρακομβικής και η ενδοκομβική περιοχή. Ο διαχωρισμός αυτός εξασφαλίζει τη γρήγορη μετάδοση των δυναμικών ενέργειας κατά μήκος των αξόνων. Κάθε μία από τις περιοχές αυτές, χαρακτηρίζεται από πολύ-πρωτεϊνικά σύμπλοκα μεταξύ τασο-ελεγχόμενων ιοντικών διαύλων, μορίων κυτταρικής συνάφειας, πρωτεϊνών-μέλη της οικογένειας Neurexin και κυτταροσκελετικών πρωτεϊνών. Το μόριο κυτταρικής συνάφειας TAG-1 (Transient Axonal Glycoprotein-1) ανήκει στην υπεροικογένεια των ανοσοσφαιρινών, εκφράζεται τόσο από τα νευρικά όσο και από τα εμμύελα γλοιακά κύτταρα, ενώ βρίσκεται στην εγγύς της παρακομβικής περιοχή των ινών του κεντρικού και περιφερικού νευρικού συστήματος. Η TAG-1 σχηματίζει ένα σύμπλοκο με την πρωτεΐνη Caspr2 της οικογένειας Neurexin και τους τασοελεγχόμενους διαύλους καλίου (VGKCs). Πιο συγκεκριμένα η TAG-1 ανήκει στην υποοικογένεια των Contactin που χαρακτηρίζεται από τέσσερις επαναλήψεις φιμπρονεκτίνης τύπου III (FNIII) και έξι Ig περιοχές. Έως τώρα, έχει δειχθεί ότι η TAG-1 αλληλεπιδρά ομοφιλικά με τον εαυτό της *in trans* μέσω των FNIII υποπεριοχών της. Επιπλέον, αλληλεπιδρά ετεροφιλικά *in cis* με την Caspr2 και τους VGKCs μέσω των Ig υποπεριοχών της, ενώ οι FNIII υποπεριοχές δε λαμβάνουν μέρος στην αλληλεπίδραση αυτή. Η μελέτη αυτών των αλληλεπιδράσεων έχει ιδιαίτερα μεγάλη σημασία καθώς η απουσία είτε της TAG-1 είτε της Caspr2 οδηγεί σε καταστροφή του συμπλόκου της εγγύς της παρακομβικής περιοχής και επακόλουθη διάχυση των VGKCs στους ενδοκόμβους. Σε μία πληθώρα απομυελινωτικών παθολογιών στις οποίες συμπεριλαμβάνεται η Πολλαπλή Σκλήρυνση, η μοριακή αρχιτεκτονική των εμμύελων ινών διαταράσσεται, κάτι που οδηγεί σε εκφυλισμό των αξόνων.

Στο πρώτο μέρος της παρούσας εργασίας, αναλύσαμε τις υποπεριοχές της TAG-1 που συμμετέχουν στην αλληλεπίδρασή της με την Capsr2, ενώ μελετήσαμε το ρόλο μιας διαλυτής μορφής της TAG-1 σε αυτή την αλληλεπίδραση. Τα αποτελέσματά μας ήταν αντιφατικά με ό,τι είχε δειχθεί, καθώς σχεδόν όλες οι υποπεριοχές της TAG-1 που ελέγθηκαν, συμπεριλαμβανομένων των FNIII, μπορούσαν να αλληλεπιδράσουν με την Capsr2. Επιπλέον, δείξαμε για πρώτη φορά ότι η πρωτεΐνη Semaphorin6A και οι ισομορφές 140 και 155 των Neurofascin αλληλεπιδρούν με την TAG-1.

Στο δεύτερο μέρος της εργασίας, έγινε μία προσπάθεια περεταίρω μελέτης του ρόλου της TAG-1 στη μυελίνωση, μέσω της χρήσης του μοντέλου Αυτοάνωσης Πειραματικής Εγκεφαλομυελίτιδας (Experimental Autoimmune Encephalomyelitis (EAE)). Απουσία της TAG-1 οδήγησε σε καθυστέρηση ανάπτυξης των νευρολογικών συμπτωμάτων, η οποία συνδεόταν με μειωμένη στρατολόγηση ανοσο-ρυθμιστικών Τ λεμφοκυττάρων (regulatory T cells) στο νωτιαίο μυελό.

A. Introduction

A.1. Myelin and Myelination

Motor, sensory and cognitive functions of the nervous system require rapid propagation of action potentials, which is facilitated by the insulation, of the majority of the axons, with the myelin sheath in vertebrates. The myelin sheath is a multilayered glial membrane that reduces the transverse capacitance and increases the transverse resistance of the axonal plasma membrane. Axons of neurons in both the Central Nervous System (CNS) and Peripheral Nervous System (PNS) are myelinated and as a result the speed of neurotransmission is increased. Rather than sweeping down an axon as a relatively slow wave of sequential membrane depolarization and repolarization, the action potential is restricted to short unmyelinated axonal segments, called nodes of Ranvier (Nave and Werner, 2014)

Through electron microscopy, the myelinated axonal segments between two nodes of Ranvier (internodes) at first glance appear similar in nerves of the CNS and PNS (Figure 1). However, the myeling-forming glial cells in the CNS are oligodendrocytes, while In the PNS are Schwann cells. These cells differ in origin (subventricular zone versus neural crest cells, respectively), the number of axonal segments per myelinating cell (1:60 versus 1:1), and the myelin periodicity (15.5nm versus 17nm). (Nave and Werner, 2014) Last but not least, the Schwann cell produces outside the myelin a basal lamina that covers totally the myelinated fiber, and is present only in the PNS. (Figure 2)

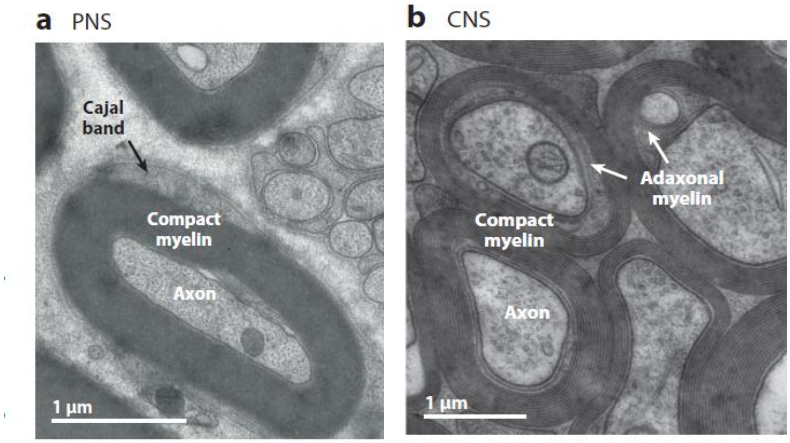

Figure 1. Myelinated axons in the PNS (a) and the CNS (b). (a) Electron microscopy of the peripheral sciatic nerve shows that a myelinating Schwann cell ensheaths one axonal segment, while in (b) the central optic nerve, oligodendrocytes myelinate multiple axonal segments (Nave and Werner, 2014)

The glial cells generally expand their plasma membrane around the axon and wrap it several times. This compact membrane is called myelin and is composed of 70-80% lipids (mainly galactosylceramide or cerebroside) and 15-30% myelin specific proteins, while it is enriched with cholesterol (Arroyo and Scherer, 2000; Saher et al., 2005). The increased composition of myelin in lipids differentiates it from other biological membranes, which have a bigger protein-to-lipid ratio. CNS myelin is composed mainly of myelin basic protein (MBP), proteolipid protein (PLP), 2':3'-Cyclic nucleotide-3'-phosphodiesterases (CNP) and myelin-

associated glycoprotein (MAG). In the PNS myelin shares some common proteins with the CNS such as MBP and MAG, while 50% of its protein texture is composed of protein P_0 and peripheral myelin protein-22 (PMP-22) follows. The only regions that do not contain compact myelin are the perinodal regions and the Schmidt-Lanterman incisures (Arroyo and Scherer, 2000).

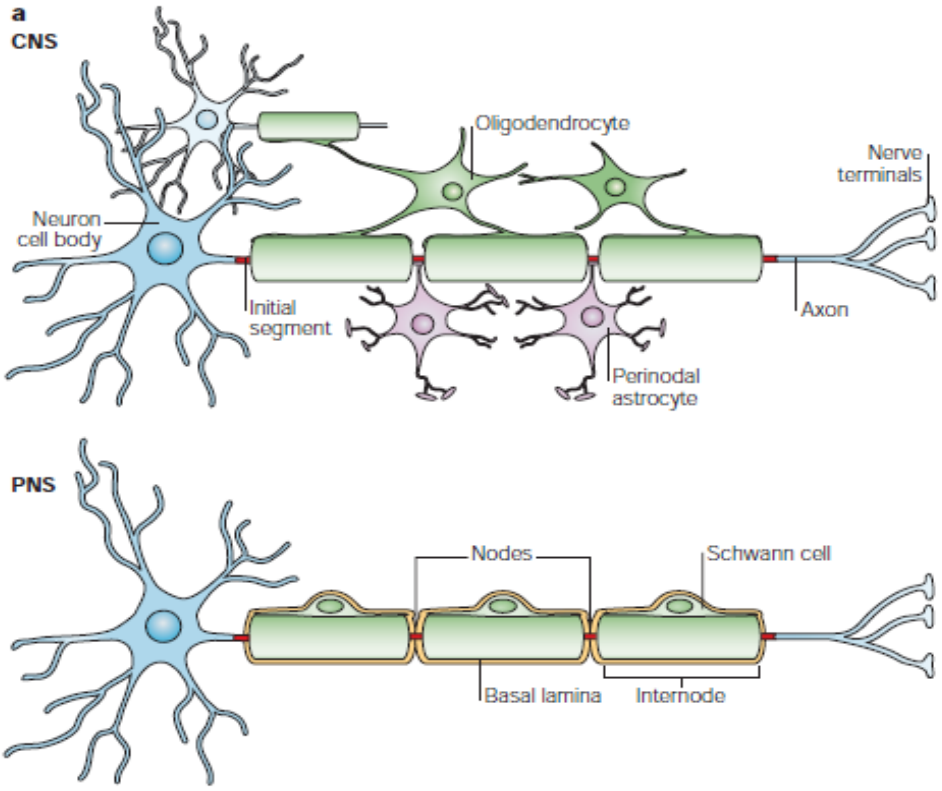

Figure 2. Structure of myelinated fibers in the CNS and PNS. The myelin sheath covers the axon at intervals (internodes), leaving bare gaps –the nodes of Ranvier. (Poliak and Peles, 2003)

The process of myelination consists of three main steps that are essential for the final formation of functional myelinated fibers. The first step concerns the selection of the axons that are going to be myelinated and the initiation of the interactions between those and the myelinating-glial cells. The next step concerns the active myelination, when the synthesis of the various myelin molecules takes place, followed by their transport towards the axon surface. Disturbance of the structural proteins of myelin (MAG, CNP, MBP or PLP) leads in destabilization of the membrane and suspension of myelination. At this step the wounding of the membrane of the glial cells around the subsequent axon takes place, forming the compact myelin. The third and final step concerns the formation of the axo-glial interactions which ensure the connection of the myelin membrane with the axon, while leaving myelin-free regions of the fibers periodically. The axo-glial interactions ensure the organization of the myelinated fibers into distinct molecular and structural domains, the function of which is necessary for the rapid propagation of the action potentials along the axon.

A.2. Axo-glial interactions

Around the nodes, glial and axonal membranes come into intimate contact, resulting in the morphologlical and functional subdivision of axonal domains. These domains are the node of Ranvier, the paranode, the juxtaparanode and the internode (Figure 3a). Each of these domains is characterized by multiprotein complexes between voltage-gated ion channels, cell adhesion molecules (CAMs), members of the Neurexin family and cytoskeleton proteins. Moreover, secreted molecules act as myelination and domain organization signals (Figure 3b). (Zoupi et al., 2011)

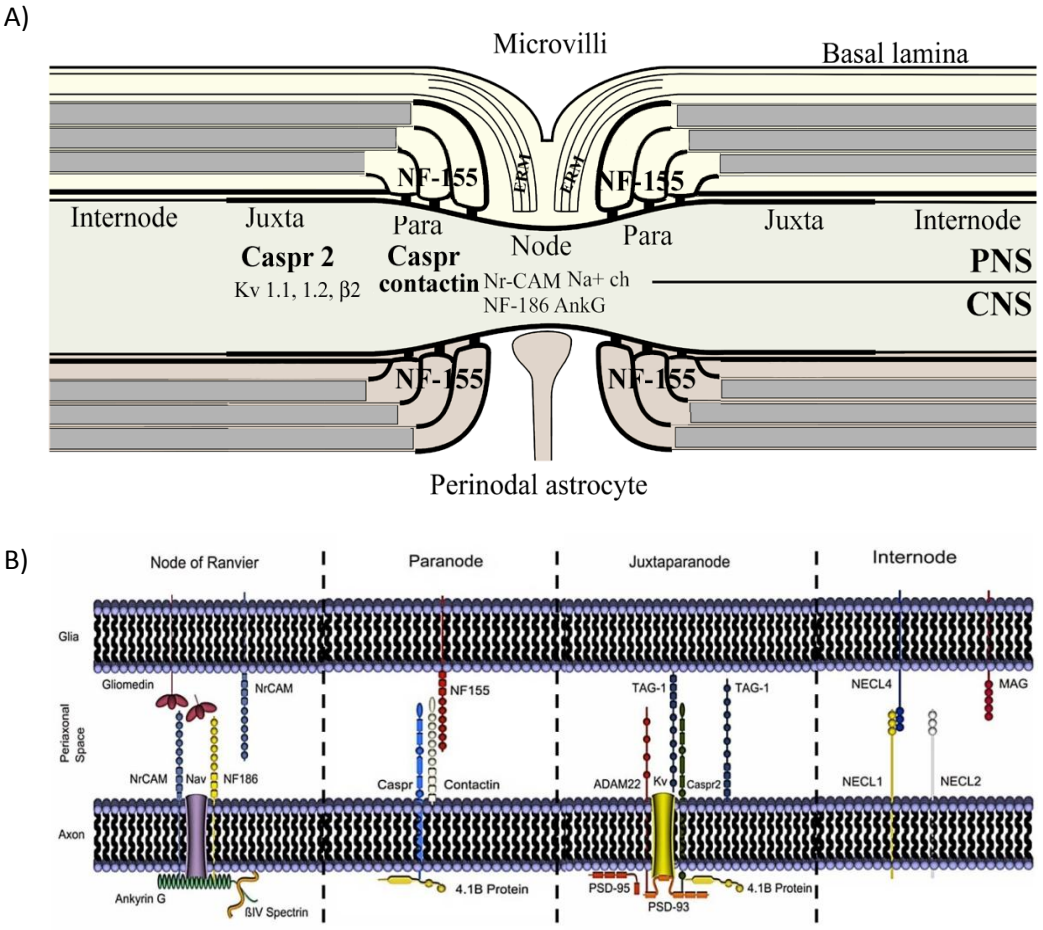

Figure 3. Organization of the domains of myelinated fibers (A) Scheme depicting the general subdivisions found on a myelinated fiber (Karagogeos, 2003) (B) Molecules found at each domain, in both the axonal and glial side in a PNS fiber (Zoupi et al., 2011)

The segregation of the myelinated fibers into distinct domains is responsible for the coordinated and the efficient function of the voltage gated sodium (Na_v) and potassium (K_v or VGKCs) channels, which are responsible for the salutatory conduction of axon potentials. The nodes of Ranvier are characterized by the accumulation of sodium channels which are responsible for the generation of action potentials. On the other hand, the VGKCs are responsible for the repolarization of the plasma membrane and are located at the juxtaparanodal region.

A.2.1 The nodes of Ranvier

As already mentioned, the only domains of myelinated fibers that are not covered by myelin are the nodes of Ranvier (~1μm-long membrane stretches between the myeliated domains of the axon) where the Na_v are retained, through interaction with the scaffold protein ankiryn-G (AnkG) (Pan et al., 2006). During development the subtype Nav1.2 is expressed while during maturation of the nodes it is replaced by the NAv1.6 (Boiko et al., 2001; Kaplan et al., 2001). Furthermore sodium channel accumulation and maintenance depend on two proteins of the L1 family of the Immunoglobulin Superfamily (IgSF). These are NrCAM, expressed by both axons and glia and the 186kDa isoform of Neurofascin (NF186), found on the axon (Feinberg et al., 2010; Zoupi et al., 2011).

A.2.2. Paranodes

The paranodal region is located between the node and the juxtaparanodal region and serves as a barrier for the segregation of sodium and potassium channels. Additionally it serves several functions, such as: to anchor the myelin to the axon and physically demarcate boundaries that limit the lateral diffusion of membrane components (Poliak et al., 1999). Morphologically, paranodes are characterized by septate-like junctions formed at axo-glial contact sites. Three molecules are implicated in paranodal junction formation. The two of them belong to the IgSF and are Contactin (Contactin-1 or Cntn-1 or F3) which is present on the axonal cell membrane and the 155kDa isoform of Neurofascin (NF155) which is detected on the glial cell membrane. The third molecule is Contactin-associated protein (Caspr), a member of the Neurexin family, containing a 4.1 binding motif in its intracellular domain. (Traka et al., 2003; Zoupi et al., 2011). In the absence of any of these molecules, paranodes are disrupted with progressive loss of axo-glial interactions, defective ion channel segregation and impaired nerve conduction (Bhat et al., 2001; Boyle et al., 2001). Contactin/F3 (a GPI-anchored protein) is essential for the recruitment of Caspr in the plasma membrane and for its targeting at the paranodal region (Boyle et al., 2001). The complex created by these two proteins interacts with NF155 (Charles et al., 2002). Thus, these three proteins are considered to form the intracellular complex that connects the glial plasma membrane with the axolemma (Girault and Peles, 2002).

A.2.3. Juxtaparanodes

The Juxtaparanodal region is adjacent to the paranodes comprising the first part of the internodal compact myelin. Its organization and maintenance depends on the combination of two distinct processes. First, the lateral diffusion barrier created by the paranodal domain and second, the formation of the juxtaparanodal membrane complex and its linkage to the cytoskeleton (Susuki et al., 2008). As in this study we will focus on the juxtaparanodal complex, a more detailed analysis of its constituents follows:

a) The cell adhesion molecule (CAM) of the IgSF, **transient axonal glycoprotein-1** (**TAG-1**/ Axonin-1/ Contactin-2; 50% aa similarity with Contactin-1), is anchored at the cell membrane through a glycophosphatodylinositol (GPI) tail, while it also exists in a secreted form (Karagogeos et al., 1991). The GPI- anchored TAG-1 is present on both the glial and axonal cell membranes (Traka et al., 2002) and will be further analyzed.

b) the Neurexin protein **Contactin associated protein 2** (Caspr2; 45% aa similarity with Caspr) (Poliak et al., 1999), which is a transmembrane protein, whose extracellular part is a mosaic of domains. Between them, are the discoidin/neuropilin and fibrinogen-like subdomains, two repeats of epidermal growth factor: EGF) and four subdomains similar to laminin A (Figure 4). Caspr2 is present only on the axonal cell membrane.
c) the **Shaker type voltage-gated potassium channels (VGKCs)**, Kv1.1 and Kv1.2 and 1.4 present only in the axonal cell membrane (Poliak et al., 2003; Traka et al., 2003).

In the absence of either TAG-1 or Caspr2 a disruption of the juxtaparanodal complex and subsequent diffusion of the VGKCs towards the internodes is observed. The role of the TAG-1/Caspr2 complex is possibly the maintenance of the VGKCs at the juxtaparanodal region (Poliak et al., 2003; Traka et al., 2003; Savvaki et al., 2008; Traka et al., 2002).

The juxtaparanodal complex is connected to the cytoskeleton through a cytoplasmic sequence of Caspr2 which allows its binding to the cytoskeletal protein 4.1B (Denisenko-Nehrbass et al., 2003; Horresh et al., 2008). The absence of 4.1B in the PNS results in disruption of the juxtaparanodal complex. (Horresh et al., 2008). Except for 4.1B, two other proteins were found to be located at the majority of the juxtaparanodal regions: the postsynaptic density protein-93/ chapsyn-110 (PSD-93) and the postsynaptic density protein 95 (PSD-95). These proteins belong in the MAGUK protein family and are able to interact through their PDZ-domain with the C-terminal of Caspr2 and the α subunit of the potassium channels (Poliak et al., 2003; Horresh et al., 2008). Reduction of both MAGUK proteins from the juxtaparanodal region does not affect neither Caspr2 nor VGKCs concerning the complex, suggesting that they are not essential for its formation (Horresh et al., 2008). Another molecule that has been recognized at the juxtaparanodal region is ADAM-22, an intracellular protein that is a constituent of the VGKC complex responsible for the connection of PDS-93 and PDS-95 scaffolding proteins at the juxtaparanodes (Ogawa et al., 2009).

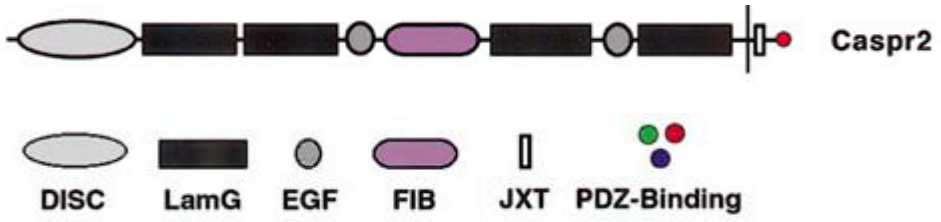

Figure 4. Structure of the intracellular protein Caspr2. DISC: discoidin-like domain, FIB: a region similar to fibrinogen, LamG: laminin G domain, EGF: Epidermal Growth Factor repeats, JXT: cytoplasmic juxtamembrane region, PDZ-binding: PSD95, DLg, ZO-1 binding domain (Spiegel et al., 2002)

A.2.4. Internodes

The internodes comprise the largest part of the myelinated fiber and this is the area of compact myelin between adjacent nodes of Ranvier. The internodal part of myelinated fibers in the PNS is characterized by small parts of looser myelin compaction, named Schmint-Lanterman incisures, which are rare in the CNS. MAG which is a member of the IgSF, is expressed in the periaxonal glial membrane by oligodendrocytes and Schwann cells, during myelination. Even though multiple interactors of MAG-1 have been identified so far, none of them seems to be crucial for the internodal axo-glial interactions. Nectin like family of adhesion molecules (Nec1 proteins) members have been recently identified to be key regulators of the internodal domain organization (Zoupi et al., 2011).

A.3. Cell adhesion molecules (CAMs)

CAMs play important roles in various cellular processes, such as cell growth and differentiation, immune response and signal transmission from the outside into the inside of the cells. CAMs are separated in 4 main protein families: integrins, cadherins, selectins and IgSF (Hynes et al., 2000).

When first discovered, neural CAMS which are expressed form the developing axons (Katidou et al., 2008), were considered to just offer to the cell surface different adhesion attributes. The following decades, it was found that these proteins are implicated in complex procedures such as axon guidance, neuronal migration, neural outgrowth and fasciculation, formation of synapses, plasticity and more recently the maintenance of the myelinated fibers integrity (Karagogeos, 2003).

A.3.1. Neural IgSF CAMs

The IgSF CAMs consists of membrane glycoproteins that are not dependent on calcium ions. The characteristic of the members of this family is the extracellular part that contains repeats that resemble with the stable region of immunoglobulins, C2 (Ig-like domains), which are connected with bisulfide bonds (Williams et al., 1988). Neural CAMs of the IgSF are known for the regulation of adhesion, neurite outgrowth and migration. IgSF represents one of the biggest superfamilies of the human, fly and worm genomes. Some of the members of this family except for the Ig-like modules (usually 4 to 6), contain a number of subdomains that resemble to fibronectin type-III (FNIII-like). This category of proteins is further divided in intracellular and GPI-anchored to the cell membrane proteins.

The first members of the IgSF neural CAMs are glycoproteins L1 (or NgCAM) and NCAM (Neural Cell Adhesion Molecule), which are distinct members of the respective subfamilies The molecules neurofascins and NrCAM belong to the L1 subfamily and take part in the axo-glial interactions. Various alternative transcripts are derived from the neurofascin gene, while the most important are those giving the products NF155, NF186 and NF140. These proteins are transmembrane and contain 6 Ig-like modules as well as FNIII-like domains. Concerning the NF155 one FNIII-like domain is absent, which is a domain that resembles the mucins proteins of metazoa. NF155 is expressed only from the glial cells. On the other hand, NF186 is expressed only by neuronal cells while NF140 is expressed only at neurons during

embryonic development. Furthermore, NF140 lacks the mucin and FNIII5 domains characteristic of NF186 or the FNIII3 domain unique to NF155 (Zhang et al., 2015; Sherman et al., 2005).(Figure 5)

Another small family of the neural IgSF CAMs is Necl (Nectin-like or SynCAm or Cadm) which contain 3 Ig-like modules, a transmembrane domain and a cytoplasmic region.

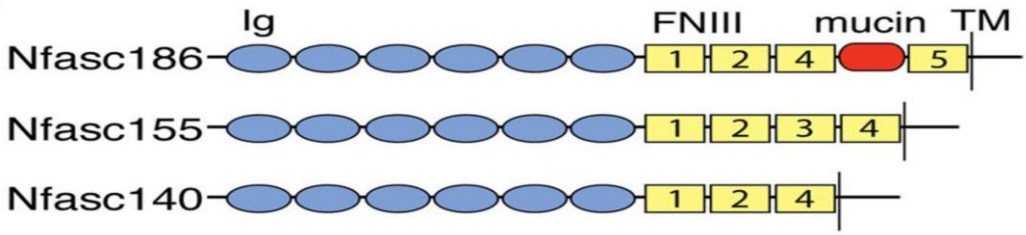

Figure 5. The domain structure of the Neurofascin isoforms. Ig, Immunoglobulin-like domain; FNIII, fibronectin type-III domain; TM, transmembrane domain. (Zhang et al., 2015)

The two main sub-groups of the GPI-linked CAMS are the Contactins and IgLON subfamilies. The members of Contactins, on which we focus in this study, are characterized by sequential homology and share some common structural characteristics. These include the same number of Ig-like modules (six) at their extracellular N-terminal, which are followed by four FNIII-type repeats and a GPI-anchor at their C-terminal through which they anchor in the cell membrane (Figure 6).

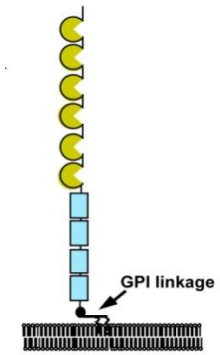

Figure 6. Structure of GPI-CAMs of the IgSF. The semicircles represent the Ig-like modules, while the rectangles represent the FNIII-type repeats (Karagogeos, 2003)

The Contactin subfamily consists of six members in total (Table 1), which are the protein contactin (or F3), the protein TAG-1 (or contactin-2 or TAX-1 in human or axonin-1 in chicken) and the proteins BIG-1, BIG-2 and NB-2, NB-3. (Karagogeos, 2003)

Human	**Rodent**	**Avian**
Contactin-1 or CNTN1	F3/contactin	F11
Contactin-2 or CNTN2 or hTAG-1 or TAX-1	TAG-1	Axonin-1
Contactin-3 or CNTN-3	BIG-1	
Contactin-4 or CNTN-4	BIG-2	
Contactin-5 or CNTN-5	NB-2	FAR-2
Contactin-6 or CNTN-6	NB-3	

Table 1. The members of the contactin subfamily and their homologues in human, rodent and avian.

A.3.2. TAG-1/ axonin-1/ Contactin-2 (or TAX-1 or hTAG-1)

In this study we will focus on TAG-1 which, as already mentioned, plays an important role in the formation of the juxtaparanodal complex. TAG-1 is a highly conserved protein whose molecular weight is ~135kDa.

TAG-1interacts in a homophilic way with itself *In trans*, as the axonal TAG-1 interacts with the glial TAG-1 through its FNIII-repeats (Tsiotra et al., 1996). On the contrary, axonal TAG-1 interacts in a heterophilic way, *in cis* with Caspr2 and VGKCs, which are located on the axonal membrane, through its Ig-like modules (Tzimourakas et al., 2007). (Figure 7) Nevertheless it was shown that glial TAG-1 physically interacts with Caspr2 (*in trans*) and is sufficient for the formation of the Juxtaparanodal complex (Savvaki et al., 2010). Heterophilic interactions of TAG-1 have been found to take place with other transmembrane proteins of the IgSF, such as L1, NrCAM, NCAM and other adhesion molecules such as Tenascin C, and phosphacan (Pavlou et al., 2002).

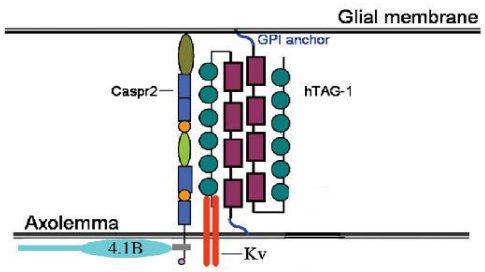

Figure 7. Schematic representation of the hypothetical interactions taking place at the juxtaparanodal complex (Tzimourakas et al., 2007)

The crystal structure of the first four Ig subdomains of TAG-1 indicates that they are compact and U shaped due to contact between subdomains 1 and 4 and between subdomains 2 and 3. In the crystals, the Ig1-4 subdomains of TAG-1 are placed in an antiparallel orientation, suggesting that the TAG-1 mediated adhesion between two cells, includes the formation of a linear zipper-like array in which TAG-1 molecules are alternatively provided by two apposed membranes (Figure 8). (Freigang et al., 2000)

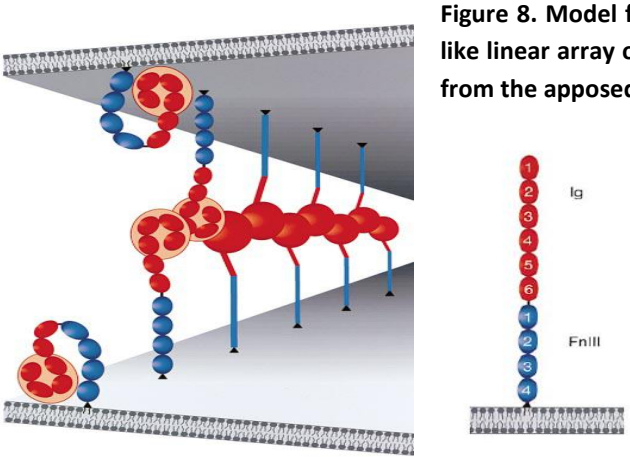

Figure 8. Model for cell-cell adhesion mediated by a zipper-like linear array of TAG-1 molecules originating alternatively from the apposed membranes (Freigang et al., 2000)

The first cDNA libraries encoding TAX-1, which is the orthologous protein of TAG-1 in human were created from Tsiotra et al., 1993. Human TAG-1 presents a high degree of homology

(91%) with the rodent TAG-1 and a lesser degree of homology (75%) with the avian TAG-1 (axonin-1). As already mentioned, the number of the IgC2 subdomains and the FNIII-type repeats that are present in TAG-1 is conserved between the three species. The higher degree of conservation concerns the second IgC2 subdomain (98% when compared to rodents and 82% when compared to avian). The human orthologue additionally contains one N-terminal signal sequence and a C-terminal hydrophobic sequence (GPI). Furthermore, TAG-1 and TAX-1 share an RGC tripeptide, a motif known for its mediation in the recognition of fibronectins and integrins. Finally, it was found that the gene encoding TAX-1 is found at the 1q32 chromosome (Tsiotra et al., 1993) and that the upstream sequence of the gene includes components that result in expression which is restricted to the nervous system, *in vivo* (Denaxa et al., 2003).

The expression of TAG-1 is highly regulated in the developing brain and is mainly located at the olfactory bulb, the neocortex, the hippocampus etc. (Wolfer et al., 1998; Yoshihara et al., 1995; Denaxa et al., 2001). During development TAG-1 takes part in a complicated circuit of interactions and controls the adhesion of neuronal cells, the migration of neuronal cells, the neurite outgrowth as well as the axon pathfinding (Karagogeos, 2003).

In the adult rodent brain, high levels of TAG-1 expression is observed in the granular layer of the cerebellum, in the pyramidal cells of the CA1 and CA3 of the hippocampus (Yoshihara et al., 1995; Wolfer et al., 1998). The main role that has been described for TAG-1 in the adult nervous system concerns the organization of the juxtaparanodal complex. Muscles lacking the gene that encodes TAG-1 (*Tag-1*$^{-/-}$) are unable to organize this complex (Poliak et al., 2003; Traka et al., 2003).

Tag-1$^{-/-}$ mice show hypomyelination in the optic nerve and selective loss of small caliber axons, loss of Caspr2 and VGKC diffusion towards the internode (Traka et al., 2003; Chatzopoulou et al., 2008; Savvaki et al., 2008). In addition, *Tag-1* null mice exhibit hypersensitivity to convulsive stimuli and reduced performance in behavioral tests for learning and memory (Savvaki et al., 2008).

Last but not least, two other facts that highlight the importance of TAG-1 are that 1) it was identified as an autoantigen in a subset of Multiple Sclerosis (MS) patients targeted by T cells and autoantibodies (Derfuss et al., 2009) and 2) it was found to be a tissue-restricted antigen (TRA), normally expressed by thymic epithelial cells (Alvarez et al. 2015).

A.4. Demyelination and Remyelination in the CNS

In the adult nervous system, the damage and progressive loss of the myelin sheath results in the demyelination of the fibers, meaning the stripping of the axon from the surrounding myelin and progressive axonal degeneration. This is a characteristic of many demyelinating diseases and one of the most common demyelinating diseases of the CNS in human is Multiple Sclerosis (MS). MS is a chronic autoimmune, inflammatory, neurodegenerative disease of the CNS, characterized by multifocal demyelinated plaques, axonal loss and glial scar formation (Lassmann, 1998). This disease affects over 2 million young adults worldwide and displays a high degree of heterogeneity in both clinical and pathologoanatomical symptoms. Even though the pathophysiology and cause of the disease are still unknown, it is

considered a disease of the CNS that affects mainly the white matter (WM). However recent data have shown that it also causes lesions in the gray matter (GM) (Ruzman et al., 2012).

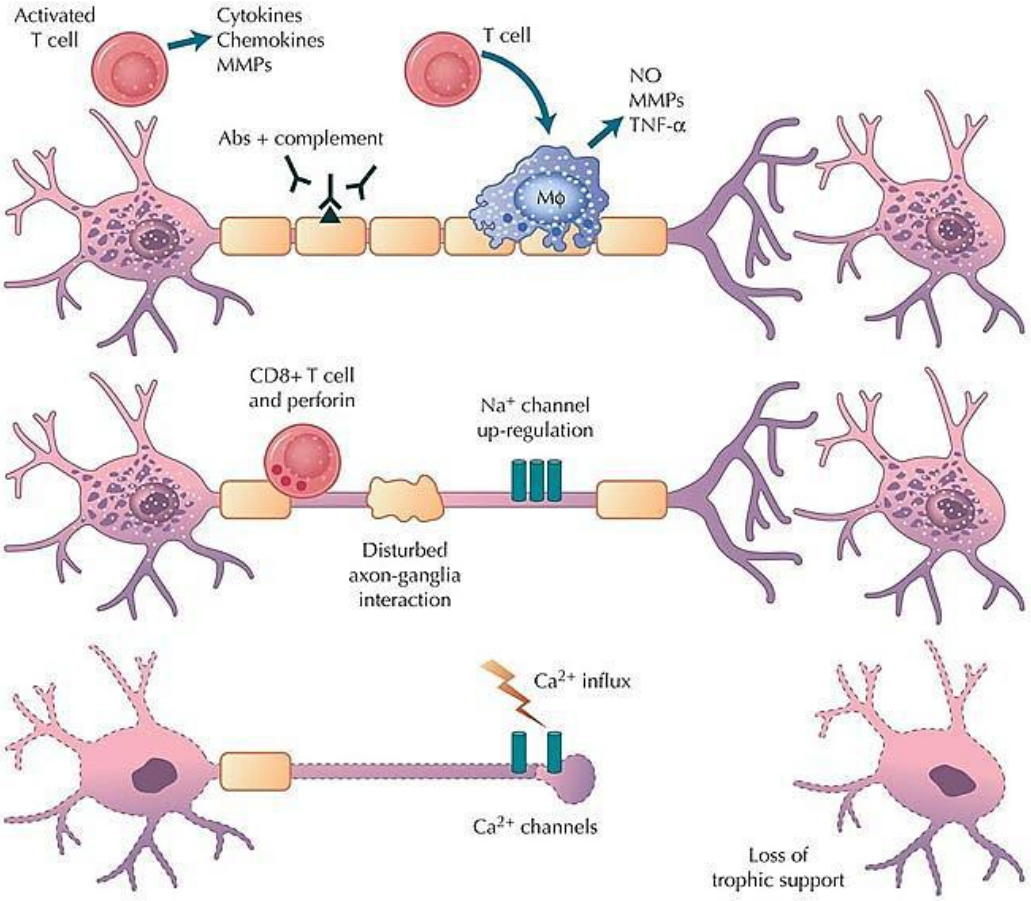

Figure 9. Stages of the immune response against the proteins of the myelin sheath and their progressive degeneration (http://mult-sclerosis.org)

There is a general assumption that MS appears in people with a genetic predisposition after their exposure to an environmental factor. This results in the activation of specialized T-lemphocytes of the periphery against to antigens of the myelin sheaths or to the myelin-producing oligodendrocytes (Figure 9). Activated T-lymphocytes disrupt the Blood Brain Barrier (BBB), invade the WM of the CNS and with the co-operation of the endogenous immune system of the brain (microglia, macrophages) they initiate an immune response against myelin. This phenomenon results in neuronal degeneration and generation of chronic demyelinating plaques (Barnett et al., 2009; Handerson et al., 2009). It should be mentioned however, that the neuronal and axonal loss observed in MS can be caused by either direct or indirect attack, as recent data describe cases of neuronal degeneration in the absence of demyelination (Nikic et a., 2011; Rudick and Trapp, 2009).

Despite the extensive damage of the myelin sheath, frequently the CNS has the ability of partial recovery of the damage, through a process named remyelination. This is possible through the activation of previously inactive oligodendrocyte precursor cells (OPCs) which are differentiated into mature oligodendrocytes that are able to produce myelin. However,

the myelin sheath that is produced during remyelination is thinner (Stassart et al., 2013). In some cases remyelination fails and this results in progressive axonal degeneration (Figure 10).

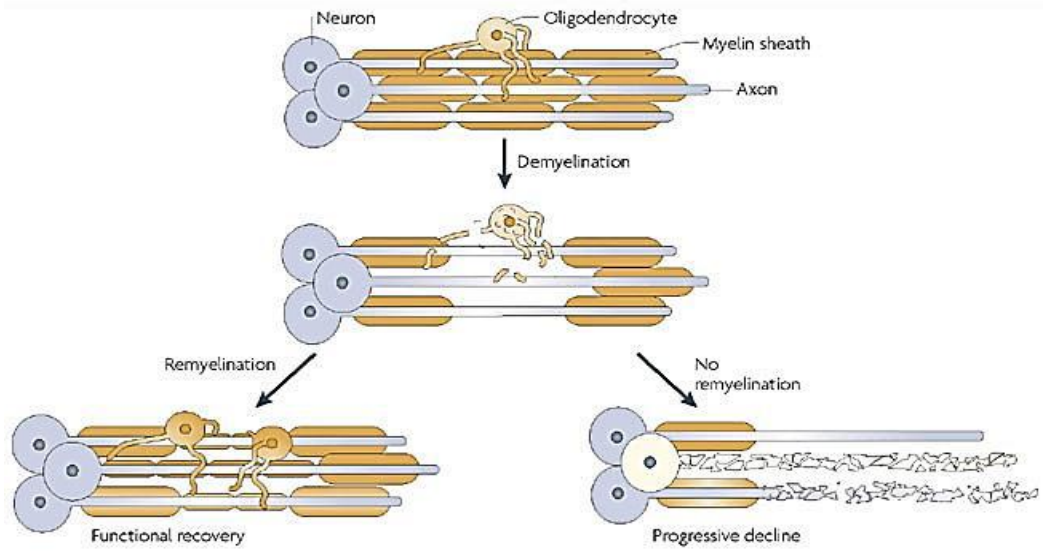

Figure 10. Schematic representation of the possibilities that follow the demyelination of the myelinated fibers (Franklin and French-Constant, 2008)

A.4.1. The pathology of Multiple Sclerosis (MS)

Despite the heterogeneity of the disease, MS can be classified into three categories based on the symptoms of the patients: relapsing remitting (RRMS), primary progressive (PPMS) and secondary progressive (SPMS). RRMS represents 85% of all cases and is characterized by repetitive incidents of increasing neurological symptoms accompanied by periods of partial recovery. The majority of RRMS cases usually progress to SPMS in 6-10 years from the disease onset, where symptom severity becomes gradually greater and there are no remissions. PPMS is the most aggressive form of MS, with initial occurrence of symptoms that lead to gradually progressive disability (Linberg and Kappos, 2006). Among the pathological hallmarks observed, are the presence of activated microglia, a compromised BBB and increased glutamate concentration (Tisell et al., 2013). MS is considered a T-cell driven disease characterized by high complexity. Infiltrates detected in lesions are mainly composed of CD8+ T-cells while CD4+ T-cells (Serafini et al., 2004).

Current therapies target the suppression of the immunological response and neuroscientists aim in unraveling the secrets of effective remyelination after an attack and neuroprotection. Although the cause of MS is enigmatic, it is believed that the neuronal and axonal loss caused by chronic inflammation and generalized immune system activation in the CNS seem to lead to the observed neurological decline (Steinman et al., 2003). There is evidence suggesting that both genetic and environmental components contribute to MS (George et al., 2016). Even though there are some common features among patients with MS, both the clinical and pathological symptoms vary, rendering MS a really heterogeneous disease involving mechanisms of initiation and progression that remain obscure.

A.4.2. Disruption of perinodal regions in demyelination and MS

In MS lesions, disorganization of nodal, paranodal and juxtaparanodal components has been reported. More specifically, in early active demyelinating lesions, the paranodal molecules NF155 and Capsr are found in elongated clusters, while VGKCs overlap with the paranodes due to their diffusion towards nodal areas (Coman et al., 2006). In chronic inactive lesions, paranodal Caspr is completely absent in the lesions and diffuse in the perilesions, where juxtaparanodal Caspr2 and VGKCs appear diffused as well. It was recently shown in two different rodent models that during demyelination, initially the paranodes elongate with subsequent juxtaparanodal components diffusion and down-regulation at the protein level. During remyelination, however, the paranodes were found to form again followed by the juxtaparanodes at later stages (Zoupi et al., 2013). Moreover, it was recently found that the molecular organization and maintenance of the juxtaparanodes is affected in lesions, perilesions and normal appearing white matter (NAWM) in chronic MS. TAG-1 clustering at the juxtaparanodes was reduced in NAWM; TAG-1 and Caspr2 are diffused in perilesions and are absent in lesion areas (Kastriti et al., 2015). Finally it is worth mentioning that autoantibodies against nodal CAMs such as Neurofascin and TAG-1 were detected in MS patients (Derfuss et al., 2009; Mathey et al., 2007).

A.5. Experimental autoimmune encephalomyelitis (EAE) mouse model of demyelination

The suggested etiologic heterogeneity of MS and the need of unraveling the disease mechanisms in order to test potential therapies are reflected by the abundance and diversity of experimental animal models of demyelination. Among them are genetic, toxic, virus-induced and immune-mediated models. Unfortunately, no demyelinating mouse model perfectly mirrors all aspects of MS either in the complexity or in all mechanisms as each one of them shows only particular similarities to its pathophysiology (Ransohoff, 2012). Undoubtedly though, they are useful in order to answer specific questions about the pathogenesis of the disease, to examine the mode of action of potential therapies and to address the role of specific proteins in remyelination.

The most commonly used model is that of the Experimental Autoimmune Encephalomyelitis (EAE) which resembles the immunological. The EAE model is an artificially-driven autoimmune model the histopathology of which mimics that of MS in several aspects, such as that it is a T-cell-driven disease and that these cells are auto reactive against myelin components (i.e. MBP, MOG and PLP) (Steinman et al., 2006; Croxford, et al. 2011). A basic difference between EAE and MS is that in the C57BL/6 mouse strain the disease is induced by a harsh induction and is monophasic, while MS is spontaneous and dynamic. Additionally in EAE lesions are found only in the spinal cord WM and are mostly dominated by CD4+ T-cells, while MS plaques are found also in the brain, both in WM and GM and the disease is mainly CD8+ T-cell-driven (Huseby et al., 2001). On the other hand EAE has greatly contributed to the understanding of basic MS pathology and importantly one drug currently widely used in MS was developed thanks to observation derived from EAE research (Yednock et al., 1992).

A.6. Aim of the study

This study consists of two main research parts:

As already analyzed, the precise distribution of ion channels at the nodes of Ranvier and the perinodal regions is critical for the efficient propagation of axon potentials along myelinated axons. TAG-1 and Capsr2 are cell adhesion molecules required for the clustering of VGKCs at the juxtaparanodes and in the absence of either of these molecules we end up with diffusion of VGKCs towards the internode. Moreover we have shown that mouse models of demyelination have disrupted VGKC clustering that does not re-organize in chronic EAE.

As it is known that TAG-1 interacts directly with both Caspr2 and VGKCs, we are convinced that understanding the functional interaction between these molecules is of high importance and may contribute to the development of clinical strategies towards the restoration of axonal disorganization in MS.

1) A) The first aim of this work is to analyze the molecular interactions between the molecules of the juxtaparanodal complex, and more specifically between TAG-1 and Caspr2, and to identify the specific regions that are implicated in this interaction.

   B) Furthermore, another aim of this study is to identify other potent interactors of the proteins that are present in the juxtaparanodal complex. This is achieved through the use of UniReD, a novel bioinformatic tool created by our collaborators in the lab of Prof. Iliopoulos, and subsequent verification of its results concerning the potent interactors of TAG-1.

2) Another goal in our lab is to examine the possible vulnerability of mice lacking TAG-1 in de- and re-myelination. For this purpose, the EAE mouse model was used in order to examine possible differences concerning demyelination, axonal loss and infiltration levels during acute and chronic EAE. Last but not least, we started to address the direct activation of the immune system in EAE-induced TAG-1 null mice.

B. Materials & Methods

B.1.1. Deletion Plasmid constructs generation

Previously in the lab, DNA clones for human TAX and its signal peptide (SP) sequence were obtained as PCR products from a construct containing the full-length cDNA sequence of the gene in pBluescript II KS (#277). First, pEGFP-C1 (Clontech) plasmid vector was manipulated to contain the signal peptide (SP) sequence of human TAX cDNA (pEGFP-C1/SP) which was obtained with PCR using the following primers: 1. Forward (NheI) 5'CTAGCTAGCATGGGGACAGCCACCAGG-3', 2. Reverse (AgeI) 5'CGACCGGTGCGGCTGAACTCCAAGCTGA-3'. The product was cloned at NheI/ AgeI restriction sites upstream of the EGFP fragment in the pEGFP-C1 vector, resulting in the generation of pEGFP-C1/SP construct (#620). Afterwards, human TAX (sequence downstream of the signal peptide sequence) was obtained with PCR (from #277) using the following primers: 1. Forward (XhoI) 5'-CCGCTCGAGCCCTGGGATCCCAAACCACC-3' and 2. Reverse (HindIII) 5'-CCCAGGCTTTCAGAGCTCCAGGGAGCC-3'. The PCR product was cloned downstream of EGFP fragment in XhoI/ HindIII restriction sites of pEGFP-C1/SP resulting in the **hTAX-1 in pEGFP-C1/SP (#621)** expressing vector (described in more detail in Salata Efi's diploma thesis). Following the same approach, the following deletion plasmid constructs were produced:

#622: Ig1-5 subdomains in pEGFP-C1/SP were obtained with PCR (from #151, IgC2 in pRMHa/RI-Hinc3, this construct already contained the GPI anchor downstream of the Ig subdomains) using the following primers: Forward (TAX354 XhoI) 5'-CCGCTCGAGCCCTGGGATCCCAAACCACC– 3' and Reverse (TAX3392 HindIII) 5'-CCCAGGCTTTCAGAGCTCCAGGGAGCC-3' (described in more detail in Salata Efi's diploma thesis, 2013).

#623: FN1-4+GPI subdomains pEGFP-C1/SP were obtained with PCR (from #277) using the following primers: Forward (FN3 2088XhoI) 5'- CCGCTCGAGCCCCGCCAGGTCCCCCAGGA-3' and Resverse (TAX3392 HindIII) 5'-CCCAGGCTTTCAGAGCTCCAGGGAGCC-3' (described in more detail in Salata Efi's diploma thesis, 2013).

#631: Ig1-4 + GPI subdomains in pEGFP-C1/SP. Firstly the Ig1-4 subdomains were obtained with PCR (from #277) using the following primers: Forward (TAX354 XhoI) 5'-CCGCTCGAGCCCTGGGATCCCAAACCACC– 3' and Reverse (TAX 1508 HindIII) 5'-CCCAAGCTTTTGCACGGCTAGCTCGGCG-3'. Downstream to the Ig1-4 sequence the GPI sequence was cloned at HindIII/XbaI restriction sites after PCR with primers: Forward (GPI-R-3392-XbaI) 5'GCTCTAGATCAGAGCTCCAGGGAGCCTA-3' and Reverse (GPI-R-3392-XbaI) 5'-GCTCTAGATCAGAGCTCCAGGGAGCCTA-3' (described in more detail in Fakoureli Eirini's diploma thesis, 2014).

#632: Ig1-6 + GPI subdomains in pEGFP-C1/SP: Firstly the Ig1-6 subdomains were obtained with PCR (from #277) using the following primers Forward (TAX354 XhoI) 5'-CCGCTCGAGCCCTGGGATCCCAAACCACC– 3' and Reverse (TAX 2087 HindIII) 5'-CCCAAGCTTACCTCGGACCAGGACTGTGG-3' Downstream to the Ig1-6 sequence the GPI sequence was cloned at HindIII/XbaI restriction sites after PCR with primers: Forward (GPI-R-

3392-XbaI) 5'GCTCTAGATCAGAGCTCCAGGGAGCCTA-3' and Reverse (GPI-R-3392-XbaI) 5'-GCTCTAGATCAGAGCTCCAGGGAGCCTA-3' (described in more detail in Fakoureli Eirini's diploma thesis, 2014).

#633:Ig1-2 + GPI subdomains in #631: The Ig1-4 subdomains were replaced by Ig1-2 at restriction sites XhoI/HindIII while the GPI anchor was already downstream of the HindIII restriction site: Firstly the Ig1-2 subdomains were obtained with PCR (from #277) using the following primers: Forward (TAX354 XhoI) 5'- CCGCTCGAGCCCTGGGATCCCAAACCACC– 3' and Reverse (TAX 983 HindIII) 5'-CCCAAGCTTTGCAAAGAGCCGGGTATCTTGAG-3' (described in more detail in Fakoureli Eirini's diploma thesis, 2014).

#634: Ig3-4 + GPI subdomains in #631: The Ig1-4 subdomain were replaced by Ig3-4 at restriction sites XhoI/HindIII while the GPI anchor was already downstream of the HindIII restriction site: Firstly the Ig3-4: subdomains were obtained with PCR (from #277) using the following primers: Forward (TAX-943F-XhoI) 5'- CCGCTCGAGCCAGCAAGTTTGCTCAGCTCA– 3' and Reverse (TAX 1508R-HindIII) 5'-CCCAAGCTTTTGCACGGCTAGCTCGGCG-3' (described in more detail in Fakoureli Eirini's diploma thesis, 2014).

#670 (new deletion plasmid construct): Ig5-6+FN1-2 + GPI subdomains in #631: The Ig1-4 subdomains were replaced by Ig5-6+FN1-2 at restriction sites XhoI/HindIII. Firstly the Ig5-6+Fn1-2 subdomains were obtained with PCR (from #277) using the following primers: Forward (TAX-1F-1508 XhoI) 5'- CCGCTCGAGCACTCGCCCCTGACTTCAGG– 3' and Reverse (TAX-1R-2696 HindIII) 5'- CCCAAG CTTCTCAGCTGAGTACACGAGTGC-3'

The plasmid construct of hCaspr2 in pcDNA in XL-iBlue MaF (#330) had been previously produced in the laboratory, while mouse Sema6A-c-myc epitope in pCX plasmid was a kind gift from Dr Alain Chedotal, INSERM U968, Vision Institute, Paris, France) and mouse Nfasc140FLAG in pCMVTag4 and rat Nfasc155FLAG in pCMVTag4 plasmids were kind gifts from Dr Peter Brophy, Centre for Neuroregeneration, Chancellor's Building, University of Edinburgh.

The #670 (Ig5-6+FN1-2 + GPI subdomains) hTAG-1 deletion plasmid construct was produced during this study and a brief description of this procedure follows:

Firstly the Ig5-6+Fn1-2 subdomains were obtained with PCR (from #277) using the following primers: 1. Forward (TAX-1F-1508 XhoI) 5'- CCGCTCGAGCACTCGCCCCTGACTTCAGG– 3' and 2. Reverse (TAX-1R-2696 HindIII) 5'- CCCAAG CTTCTCAGCTGAGTACACGAGTGC-3'

The PCR conditions were:
Volumes used for PCR reaction:
1µl DNA template #277 (1µg/µl)
1.5µl dNTPs 10mM
10µl 5x KAPA HiFi buffer with Mg^{2+}
4µl Primer F (c=25ngram/µl)
4µl Primer R (c=25ngram/µl)
1µl KAPA HiFi DNA polymerase
28.5µl dH_2O

PCR Program:

Initial denaturation : 95°C for 3min, 1cycle

- **Denaturation**: 98°C for 20 sec
- **Annealing**: 65°C for 15 sec
- **Extension**: 72°C for 90 sec

} 32 cycles

Final extension: 72°C for 3 min, 1 cycle
Final temperature: 4°C, ∞

The product from this PCR was then digested with the restriction enzymes XhoI and HindIII of New England Biolabs.

In order to replace the Ig1-4 subdomains by the Ig5-6+FN1-2 at restriction sites XhoI/HindIII, the #632 template was digested with the restriction enzymes XhoI and HindIII which was incubated for 3hours at 37°C:

Digestion volumes:

4μl DNA template #632 (1.4μg/μl)
5μl NEB buffer II
5μl BSA 10x
2μl XhoI (NEB)
2μl HindIII (NEB)
32μl H_2O

After the digestion with the restriction enzymes, Gel clean-up using the Nucleo Spin Extract II Gel clean-up/ Macherey-Nagel kit, followed in order to isolate the vector without the Ig1-4 subdomains. The purified vector (#632/X.H.) was then dephosphorylated with the use of the enzyme Antarctic Phosphatase of NEB:

Volumes used for the dephosphorylation process:
8μl #632/X.H. vector
1μl 10x Antarctic Phosphatase Buffer
1μl Antarctic Phosphatase-NEB

Incubation for dephosphorylation:
10min at 37 °C
6min at 65 °C
4 °C, ∞

The next step was the ligation of the #632/X.H. vector and the PCR product Ig5-6+FN1-2 that we wanted to insert between the XhoI and HindIII restriction sites.

Ligation:

2μl #632/X.H. vector
2μl PCR product Ig5-6+FN1-2/X.H.
2μl 10x ligation Buffer NEB
1μl T_4 DNA ligase NEB
13μl dH_2O

} incubation at 16°C for 3hours

Finally, transformation through electroporation of the DH10b *E.coli* electrocompetent cell line took place, which was followed by isolation of plasmid DNA through alkaline solution (mini prep) and Plasmid DNA purification through the NucleoBond Xtra Midi, Macherey-Nagel kit (Midi prep).

B.1.2. Eukaryotic cell culture

The HEK293T (Human Embryonic Kidney) eukaryotic cell line was used. For the culture of these cells the following medium was used: DMEM (Dulbecco's Modified Eagles Medium, SIGMA) supplemented with 10% FBS (Fetal Bovine Serum, GIBCO) and 100units/ml penicillin and streptomycin (GIBCO). The cells were incubated under sterile and stable conditions at 37°C and 5%CO_2. When the cells covered ~80% of the surface of the flask or the dish that was used, their separation in more flasks/dishes followed:

1) The medium that covers the cells is used and through disposable serological pipetting the cells were detached from the flask/dish surface
2) The cells are placed in 50ml tubes and centrifuged for 4' at 1200rpm.
3) The supernatant medium is removed and the cell precipitate is redissolved in a suitable medium volume
4) The cells are then parceled in new flasks/dishes and extra medium is added (~10ml final volume in 75cm^2 flask)

B.1.3. Transfection of HEK293T cells and cell lysis for obtaining protein extract

For the transfection of HEK293T cells with the TAG-1 deletion plasmids, the TurboFect Transfection Reagent (Thermo Scientific) was used, which is a sterile solution of a proprietary cationic polymer in water. Thus, the efficient plasmid delivery into eukaryotic cells is ensured. The protocol suggested from the manufacturing company was followed. Briefly:

1) 24h before the transfection 3x10^6 cells are cultured at 10cm culture dishes with 10ml medium (DMEM+10%FBS+p/s)
2) The next day if the cells cover ~70-90% of the surface the transfection can take place, after changing the medium (DMEM+10%FBS+p/s)
3) 15ug of total plasmid DNA is added (1:1 in co-transfections) in an eppendrof which is diluted with 30ul TurboFect and DMEM (serum-free) in a final volume of 1500ul
4) After being gently mixed, the dilution is incubated for 15-20min in room temperature (RT)
5) The dilution then is carefully added in the dish with the HEK293T cells

6) The cells are then incubated at 37^{o}C and 5% CO_2 for 48hours *
7) Then the dishes are placed on ice and the medium is carefully removed
8) The cells are washed with 2ml 1x PBS/dish
9) 1ml of either pyranoside lysis buffer (table 2a) or RIPA buffer (table 2b) (for the release of proteins) is added in each dish and 1min later the cells are collected, added to an eppendrof and placed on ice
10) Then cells are homogenized through sonication and kept in -20^{o}C till further processing
11) Before Immunoprecipitation (IP) or Western blot analysis the samples are centrifuged for 20minutes at 4^{o}C and 12000rpm and the supernatant is transfered in a clean tube which should always be kept at 4^{o}C
12) The last procedure is repeated until the samples have a lucid color and we get no pellet

*Note: in the case where the effect of the secreted form of TAG-1 was checked, 4hours after the transfection the supernatant medium was replaced with fresh medium and 100μg of filtered (0,20μm) secreted TAG-1 were added carefully in the 10cm well. Then the cells were incubated for another 44hours

In the case of co-transfection of HEK239T cells with human TAX in pEGFP-C1 (#621) expression plasmid and either mouse Sema6A-c-myc epitope in pCX (#674)(kind gift from Dr Alain Chedotal, INSERM U968, Vision Institute, Paris, France), mouse Nfasc140FLAG in pCMVTag4 (#671) or rat Nfasc155FLAG in pCMVTag4 (#672) (kind gift from Dr Peter Brophy, Centre for Neuroregeneration, Chancellor's Building, University of Edinburgh) , the Lipofectamine 2000 Reagent (Invitrogen, Thermo Fisher Scientific) was used. Briefly:

1) 24h before the transfection, 3x10^{6} cells are cultured at 10cm culture dishes with 10ml medium (DMEM+10%FBS+p/s)
2) The next day if the cells cover ~70-90% of the dish surface the transfection can take place: after changing the medium DMEM (serum-free) 15ug of total plasmid DNA is added (1:1 in co-transfection) in an eppendrof with OptiMEM I with Glutamax (GIBCO) medium and is gently mixed
3) In a second eppendrof 32μl of Lipofectamine and 500ul of OptiMEM I with Glutamax (GIBCO) medium were mixed
4) The content of the two eppendrofs was then mixed and incubated for 5min in RT
5) The dilution is then carefully added in the dish with the HEK293T cells
6) The cells are then incubated at 37^{o}C and 5%CO_2 for 48h in total, while the medium is replaced by fresh DMEM+10%FBS+p/s, 4h after the transfection

   Steps 7-12 follow as described above.

a) **Pyranoside lysis buffer**	
Substance	**Concentration**
Tris-HCl pH 7.5	85mM
NaCl	30mM
EDTA	1mM
Glucose	120mM
Triton X-100	1%
Octyl β-D glucopyranoside (SIGMA)	60mM
PMSF (phenylmethylsulfonyl fluoride)	1mM

b) **RIPA buffer**	
Substance	**Concentration**
Sodium chloride	150mM
Triton X-100	1%
Sodium deoxycholate	0.5%
SDS (sodium dodecyl sulfate)	0.1%
Tris, pH8.0	50mM
PMSF (phenylmethylsulfonyl fluoride)	1mM

Table 2. Pyranoside lysis buffer(a) and RIPA Buffer(b) recipes

B.1.4. Culture of Lepidoptera cells and isolation of the secreted TAG-1 protein

For the expression of the TAG-1 protein in large quantities in the supernatant medium, a cell line from *Trichoplusia ni* (lepidoptero found in cabbage) embryo was used. This cell line is named BTI-Tv-5B1-4 (or High Five ^{TM}) and is ideal for the expression of proteins. The plasmid construct for the expression of the cDNA of TAG-1 was created in the lab (rTAG-1 in the plasmid vector pIE1/153A containing the epitope Xa-Myc-6xHis) and was send to Dr K. Iatrou (E.K.E.F.E Dimokritos, Ahtens) for the production of the cell line that expressed stably the protein TAG-1 chimerically with 6 His residues.

For the culture of High Five $^{TAG-1}$ cells the ESF-AF medium from Expression Systems was used. The cells were incubated at 28^{o}C, without provision of CO_2.

For the production of protein in medium scale:

- 75cm^2 flasks are used
- In the medium the gentamycin (final concentration 50μg/ml) antibiotic is used
- A starter culture of 3x10^6 cells/flask is kept at 28^{o}C for 10 days in order for the cells to grow
- The supernatant medium containing the non-purified protein is removed in dialysis tubing membrane (12-14kDa from Medicell) and is secured with special clips.
- The membrane is then placed in hundredfold volume of 1xLEW buffer, pH 8.0 for equilibration. (1Lt 1xLew buffer: 6.9 gr $NaH_2PO_4 \cdot H_2O$ and 17.5gr NaCl are diluted in dH_2O)
- After equilibration of the solution containing the protein, the Amicon Ultra-15 centrifugal filter units (Merck Millipore) were used for condensation
- Then the protein solution was purified through Protino Ni-IDA packed columns (Macherey Nagel). The purification was performed according to the instructions of the manufacturer
- A small quantity of the purified protein was used for quantification (Bradford) and SDS-page (7.5%) for confirmation of its specificity

B.1.5. Co-Immunoprecipitation (Co-IP)

1) Protein lysates were precleared with 40ul protein G Sepharose beads (GE Healthcare LifeSciences) for 1 h at 4°C. Note: a small amount of G Sepharose beads was washed 3x with wash buffer prior to use in all steps
2) Brief spin down follows and the supernatant is separated equally in two clean tubes. The G-preclearance beads are kept at 4°C
3) Co-IP is performed by incubating the lysate with 1µg/tube of antibody overnight (O/N) at 4°C
4) The next day 40µl of protein G Sepharose beads are added in each tube and incubated for 2h at 4°C
5) Brief spin down followed and after removal of the supernatant, the G Sepharose beads (together with those of the preclearance step) are washed 3x with wash buffer
6) After the final wash, the liquid is totally removed from the beads and sample buffer with 0,1M DTT, is added to each sample
7) The samples are then boiled at 100°C and are ready for SDS-PAGE and immunoblotting

WASH BUFFER:
5mM Tris-HCl pH 8.0
1% Triton X-100
50mM NaCl
2.5mM $CaCl_2$
2.5mM MgCl

B.1.6. Western blot (WB) analysis

B.1.6.1. Quantification and sample preparation

1) In 1,5ml tube 799ul ddH_2O and 1ul from protein lysate is added, so that the final volume is 800ul
2) 200ul of Bradford (Biorad) dye are added to the sample
3) Mix through vortex
4) Incubation at RT for 15min
5) Measurement of optical density (OD) in 595nm follows
6) The quantification was carried out via the use of a standard curve resulting from the assignment of known amounts of BSA (Bovine Serum Albumin, Sigma) at the x-axis and with the values of the OD at 595nm on the y-axis
7) After calculating the total amount of protein in the sample, the desired amount is transferred to a new tube and sample buffer (1x final volume) as well as DTT (Dithiothreitol, final volume 100mM) are added to each sample.
8) The samples are then boiled at 100°C and are ready for SDS-PAGE

2x Sample Buffer:
100mM Tris-Cl pH6.8
4% SDS
0,2% bromophenol blue
20% glycerol

B.1.6.2. Protein separation with SDS-polyacrylamide gel electrophoresis (SDS-PAGE)

Protein samples prepared as described above were fractionated by 6 or 7.5% SDS-polyacrylamide gel electrophoresis (SDS-PAGE, Bio-Rad). Gels were prepared as outlined below:

Stacking gel (1 minigel 1.5mm-thick)	**Separating gel (1 minigel 1.5mm-thick)**	**6%**	**7.5%**
3.6ml dH_2O	dH_2O	5.5ml	5ml
900µl 30% acrylamide	30% acrylamide	2ml	2.5ml
1.5ml stacking gel buffer (1.5M Tris-Cl pH6.8 +0.4% SDS)	separating gel buffer (1.5M Tris-Cl pH8.8 +0.4% SDS)	2.5ml	2.5ml
60µl 10% APS (ammonium persulfate)	10% APS (ammonium persulfate)	100µl	100µl
6µl TEMED (N,N,N',N'-tetramethylethylenediamine, MERCK)	TEMED (N,N,N',N'-tetramethylethylenediamine, MERCK)	5µl	5µl

Table 3: Volumes for SDS-polyacrylamide gel preparation

- Preparation of the SDS-polyacrylamide gel (see table 3) and insertion of the gel in the electrophoresis tank as instructed by the manufacturer (Biorad)
- The electrophoresis tank is filled with 1Lt of 1x running buffer
- Prepared samples are loaded in the buffer-submerged wells, next to a commercial protein ladder
- The electrophoresis device is set to 80 V during the packing of the samples in the stacking gel (~30min)
- Afterwards the device is set to 100V until the bromophenol blue exits the gel (~2h)

10x Running-Transfer Buffer (1Lt):
900ml 10x Tris-Glycine
100ml SDS 10%

For 1Lt Running Buffer: 100ml 10x Running-Transfer buffer and 900ml ddH_2O are mixed

10x Tris-Glycine (1Lt, pH 8.3):
30,2gr Tris-base
188gr glycine

B.1.6.3. Western Blotting

1) 1x transfer buffer is prepared 1h before use, and placed at 4°C
2) One piece of 0.45 μM Protran nitrocellulose transfer membrane (GE Healthcare LifeSciences) and 6 pieces of Whattman paper (GE, Healthcare) are cut according to the dimensions of the gel and together with special sponges provided by Biorad, are presoaked in 1x transfer buffer
3) The running buffer is removed from the electrophoresis tank and the gel is isolated
4) The stacking gel is removed and only the part corresponding to the separating gel is kept
5) Firstly a sponge is placed on the black side of the "sandwich" case and 2 pieces of Whattman paper ,the gel, the nitrocellulose transfer membrane, 2 pieces of Whattman paper and another sponge follow in order. Note: a plastic pipet is used to remove air bubbles that may have stuck between the membrane and the gel
6) The sandwich is then secured and placed in the electrophoresis device, with the black side of the sandwich in the black side of the device
7) The device is filled with cold transfer buffer 1x
8) The whole tank is placed in a container filled with ice and then the device is set to 310mA for 1h to ensure the transfer of the proteins form the gel to then membrane

For 1Lt Transfer Buffer: 100ml 10x Running-Transfer buffer, 200ml methanol 100% and 700ml ddH_2O are mixed

B.1.6.4. Immunoblotting

1) The membrane is carefully removed from the apparatus and is incubated in PBSMT (0,1% PBS-Tween with 5% milk) for 1h (blocking)

0,1% PBST (500ml):
500ml 1xPBS
500μl Tween 100%

2) The membrane is then incubated with the appropriate antibody diluted in PBSMT O/N at 4°C
3) The next day the antibody is removed
4) 3x washes with 0,1% PBST, 15min each follow
5) Incubation of the membrane with the appropriate horseradish-conjugated secondary antibodies
6) 3x washes with 0,1% PBST, 15min each follow
7) Visualization of signal with enhanced chemiluminescence (ECL Plus, Amersham, GE Healthcare Bio-Sciences)

B.1.7. Embryonic brain dissection, fixation and preparation for cryosections

After the sacrifice of a wild type mouse at embryonic day 13.5 (E13.5), the embryos were collected and embryonic brain dissection followed. The brains were incubated for 12-18h in 4% PFA in 1xPBS. The embryonic tissues were then washed with 1xPBS and incubated in 30% sucrose solution in 1xPBS to allow cryoprotection. Finally, tissues were embedded in a gel consisting of 15% sucrose and 7,5% gelatin in 1xPBS and frozen in isopentane at 45^{o}C. Tissue blocks were stored at -80^{o}C prior to cryosectioning (Cryostat, LEICA). Sections of 12μm were collected on glass slides and stored at -20 ^{o}C until further processing.

B.1.8. Immunohistochemistry on cryosections from embryonic tissue

- The slides were removed from -20oC and the tissue was encircled with Dakopen.
- Washes in 1xPBS and 0.1% Triton (1xPBT) for 5 min (3x).
- Incubation in 5% Bovine Serum Albumin (BSA) and 0.1% Triton in 1xPBS (blocking solution), 1h, RT, to block unspecific binding of the antibodies.
- Incubation of the sections in primary antibody diluted in blocking solution, 12-18 hours, 4 ^{o}C
- 3xWashes in 1xPBT, 10min, RT.
- Incubation with secondary antibody diluted in blocking solution, 1-2 hours, dark conditions, RT.
- 3xWashes in 1xPBT, 10min, RT
- Mount sections with MOWIOL and store in 4oC or -20oC for longer storage.

B.2.1. Laboratory animals

One of our main goals was to study the possible vulnerability of mice lacking TAG-1 (or expressing only rTAG-1 by oligodendrocytes) to demyelinating protocols. In order to successfully induce the EAE (see section below) all animals had to belong to the C57BL6 background. For this purpose, previously in the lab, *Tag-1-/-* and *Tag-1-/-;plpTg$^{(rTag-1)38}$* mice were backcrossed in the C57BL/6 background.

B.2.1.1.Genotyping

Animals from breedings are handled at an early stage (postnatal days 5-10) and a small piece of tail is collected after they are marked according to their fingers.

B.2.1.2. Genomic DNA extraction from tail pieces

1) Each tail piece is added in a PCR tube
2) In each tail piece 40μl of Denaturating Buffer (25mM NaOH and 0,2mM EDTA pH 8.0) is added
3) Vortex follows
4) The PCR tubes that contain the tail pieces are place in a PCR machine at 98OC for 1hour in order to denaturate
5) Afterwards, 40μl of Neutralization Buffer (40mM Tris pH 8.0) is added to each tail piece

6) Vortex follows
7) The supernatant that contains the gDNA can be directly used for PCR

B.2.1.3. Genotyping PCR

In order to acquire the genotype of the animals used in this study one PCR was used to detect the wild type or knock-out band for *Tag-1* as mentioned in Fukamauchi et al. 2001 (primers "Tag-1 5'", "Tag-1 3'", "Neo 3'") and one to detect the presence or absence of *rTag-1* as follows:

- Primer "PLP internal 7846 Forward" (PLP int for):

5'-AAGGAGACTGGAGAGACCAGG-3'

- Primer "rTAG-1 143 Reverse" (rTAG-1 rev):

5'-GAATCAACTGGAGACTCAGGC-3'

The setup of each reaction and the PCR programs used are shown below:

Gene	**PCR reaction (V_{total}=20 µL)**	**PCR program**		
Tag-1	1 µL genomic DNA (gDNA)	**Step**	**Temperature**	**Duration**
	2 µL 10xTaq Buffer (Minotech)	1.	94°C	4 min
	2 µL 2 mM dNTPs	2.	94°C	30 sec
	1.3 µL of primers Tag-1 5' and 3' (stock:50 ng/µL)	3.	61°C	45 sec
	1 µL of primer Neo 3' (stock: 50 ng/µL)	4.	72°C	1 min
	1 µL 10% DMSO	5.	Repeat steps 2-4 32 times	
	0.6 µL Taq polymerase (stock 2U/µL, Minotech)	6.	72°C	5 min
	9.8 µL sterile dH_2O	7.	4°C	
PLP::rTag-1	1 µL genomic DNA (gDNA)	1.	94°C	4 min
	2 µL 10xTaq Buffer (Minotech)	2.	94°C	30 sec
	2 µL 2 mM dNTPs	3.	61°C	45 sec
	1.5 µL of each primer (stock:20 ng/µL)	4.	72°C	1 min
	0.6 µL Taq polymerase (stock 2U/µL, Minotech)	5.	Repeat steps 2-4 32 times	
	11.4 µL sterile dH_2O	6.	72°C	5 min
		7.	4°C	

In the present study the Tag-1 -/-; plp- and Tag-1 +/+; plp- were used.

B.2.2. Induction of Experimental Autoimmune Encephalomyelitis (EAE)

To assess the role of TAG-1 in demyelintation and remyelination in a model of autoimmune demyelination the MOG_{35-55}-induced EAE model (adapted from Ioannou, et al.,2012) was used. Female mice of the C57BL/6 background bred at the Animal Facility of IMBB were subjected to this protocol at 8-16 weeks of age. A brief outline of the experimental protocol is presented in Figure 12.

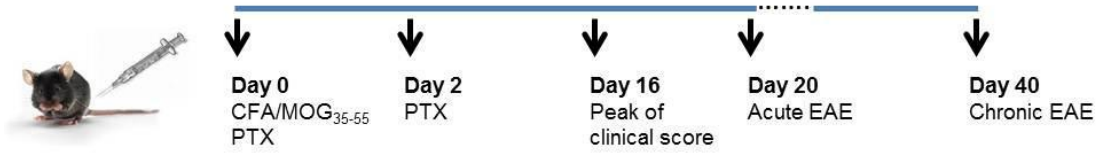

Figure 12: Schematic outline of the experimental design of EAE for 8-16-week-old female C57BL/6 mice.

In the experimental group, referred from now on as "MOG_{35-55}", on day 0 mice received a subcutaneous injection of the adjuvant at the base of their tail prepared as follows:

1. Mix in an eppendorf tube on ice:
    - 200 µg synthetic MOG_{35-55} peptide (CASLO) in 100 µL 1xPBS
    - 100 µL Complete Freund's Adjuvant (CFA, Cat. No. F5881, Sigma-Aldrich) with 4 mg/mL non-viable, desiccated *Mycobacterium Tuberculosis* H37 Ra (Cat. No. 231141, Difco Laboratories, BD Biosciences)
2. Sonication until mixture is white, stiff, viscous and of uniform consistency.

Additionally, on day 0 and day 2 mice received an intra-peritoneal injection of Pertussis Toxin (PTX, Cat. No. #181, List Biological Laboratories, Inc.) of 200 ng in 1xPBS in a final volume of 200 µL. This results in autoimmunity directed against myelin and CNS infiltration of auto reactive immune cells due to disruption of the blood-brain-barrier (BBB).

A second group of mice received the adjuvant lacking the peptide accompanied by the PTX and were used as the control group, from now on referred as "CFA". These mice present an unspecific, generalized immune reaction and BBB disruption. A third group of age-matched, naïve wild type female mice were included as a reference group.

Following injections mice were kept and monitored daily from day 7 and on until the time of sacrifice. The following clinical score scale was used to assess symptom severity:

Score	Description	Signs
0	No neurological signs	Normal behavior
1	Flaccid tail	Tail limp, lacking muscle tone
2	Hindlimb weakness or abnormal gait	Wobbly walk
3	Complete hind limb paralysis	Dragging hind limbs, abnormal righting reflex
4	Complete hind limb paralysis and fore limb weakness or paralysis	Movement in circles or only with one fore limb
5	Moribund or deceased	

In addition to the clinical scoring, body weight was also recorded daily, since it is known that disease correlates with weight loss.

B.2.3.Histological Methods

B.2.3.1. Tissue fixation, dissection and isolation

EAE-induced animals were sacrificed at 20dpi and 40dpi and the spinal cord was collected and further processed as follows:

Adult mice received an intra-peritoneal injection of anesthesia (per g of body weight: 200 μg of ketamine and 30 μg of xylazine diluted in sterile dH_2O in a final volume of 10 μL). Responsiveness to painful stimuli was checked by pinching of the tail or hind limb. After lack of response was ensured, incisures were made to expose the sternum and internal organs, the diaphragm and ribcage was cut, finally exposing the heart. A peristaltic pump was used to circulate 20-25 mL 1xPBS through the vasculature by inserting a needle in the lower wall of the left ventricle and releasing extra pressure by opening a small hole at the right atrium. Following clearance of the blood 50-60 mL of cold 4% PFA in 1xPBS were circulated to fix the tissues. The spinal cord was carefully dissected and post-fixed in 4% PFA in 1xPBS on ice, for 20-30 min.

B.2.3.2. Cryoprotection

Following post-fixation, samples are washed 3 times in 1xPBS and submerged in 10 volumes of 30% sucrose, 0.1% NaN_3 in 1xPBS. Samples are kept at 4°C until the sucrose completely replaces the intracellular water, so that the samples sink at the bottom of the container.

B.2.3.3. Embedding, freezing and cryosectioning

After cryoprotection is complete, the spinal cord was cut in 6 pieces (corresponding to 1) cervical, 2) low cervical-upper thoracic, 3) thoracic, 4) low thoracic-upper lumbar, 5)lumbar and 6) sacral) and embedded (1-3 together in one block and 4-6 together in another block) in a gel containing 15% w/v sucrose, 7.5% gelatin from porcine skin (Cat. No. G-2500, Sigma) in

1xPBS. To ensure uniform freezing, samples are submerged in methylbutane and are frozen at -35 to -40°C. Tissue blocks are then stored at -80°C before proceeding to cryosectioning (Leica). 12-µm-thick sections are collected on glass slides and stored in cryoboxes at -20°C until further processing.

B.2.3.4. Immunohistochemistry (IHC) on cryosections derived from adult tissue

Cryosections derived from CNS of adult mice were immunostained as described below:

1) Cryosections are removed from -20°C, encircled in Dako Pen (Cat. No. S200230, Dako, Agilent Technologies) and post-fixed in ice-cold acetone at -20°C for 10 min.
2) Washes (3x) in 1xPBS, 5 min each.
3) Incubation in Blocking Solution of 5% bovine serum albumin (fraction V, BSA) in 0.5% Triton X-100 in 1xPBS for 1 h, RT.
4) Incubation with the appropriate primary antibodies diluted in Blocking Solution at 4°C, overnight.
5) Washes (3x) in 1xPBS, 5 min each.
6) Incubation with the appropriate secondary fluorescently labeled antibodies (see Table) in Blocking Solution for 1.5 h, RT.
7) Nuclear counterstaining with DAPI (0.1µg/mL in dH_2O, Sigma-Aldrich), for 5 min, RT or with TO-PRO®3 iodide (500 nM in 1xPBS, Molecular Probes, ThermoFisher Scientific) for 3 min, RT.
8) Washes (3x) in 1xPBS, 5 min each.
9) Mount using mounting medium containing MOWIOL® 4-88 Reagent (Cat. No. 475904, Calbiochem, EMD Chemicals, Merck KGaA).
10) Slide storage at 4°C until imaging take place and for long term storage after it is completed.

Mounting Medium for IHC
2.6 g MOWIOL® 4-88 Reagent
6 g glycerol
12 mL Tris 0.2 M pH 8.5
6 mL dH_2O

Imaging took place using the confocal microscope TCS SP8, Leica Microsystems GmbH.

B.2.4. Quantification of immunohistochemical experiments

For the quantification of various cell types or structures in immunohistochemical experiments images were acquired using a confocal microscope (TCS SP2 and TCS SP8, Leica Microsystems GmbH) and under the same laser and detector settings for all samples.

B.2.4.1. Quantification of demyelination

Demyelinated white matter areas (WM lesions) were measured in the spinal cord of EAE-induced animals. Coronal spinal cord cryosections immunostained against PLP/NF200 were imaged with a 20x lens and 0.75 digital zoom and further processed and analyzed in ImageJ software, version ImageJA 1.45b (Schneider, et al. 2012). Lesions were marked by hand and the area was measured by the respective software tool. Demyelination was expressed as a percentage of demyelinated area over the total area of the spinal cord white matter. A minimum of 2 sections per animal in each area of the spinal cord (cervical, thoracic) was included in the quantification. Data were expressed as mean±standard error of the mean and statistical analysis was performed using the GraphPad Prism version 5.00 for Windows (GraphPad Software, San Diego, CA). Lesion area was compared between genotypes using non-parametric one-way ANOVA with Bonferroni's multiple comparison test and differences were considered as significant when $P<0.05$.

B.2.4.2. Quantification of autoimmune infiltrates

Infiltration of the spinal cord of MOG-treated animals (see section below) by immune cells was quantified in a minimum of 2 sections per animal in each area of the spinal cord (cervical, thoracic). Coronal spinal cord cryosections immunostained against MBP/IBA1 were imaged with a 20x lens and 0.75 digital zoom and further processed and analyzed in ImageJ software, version ImageJA 1.45b (Schneider, Rasband et al. 2012). Firstly, images were converted to RGB and channels were split in black-and-white. A Gaussian filter was applied to enhance signal-to-noise ratio and then a threshold was set to discriminate between postitively stained area and background. This resulted in a binary image (with single objects which were positively stained) which was analyzed using the particle analysis tool and the IBA1+ area was calculated as a percentage of the white matter, the gray matter and the total spinal cord area. Data were expressed as mean±standard error of the mean and statistical analysis was performed using the GraphPad Prism version 5.00 for Windows (GraphPad Software, San Diego, CA). Infiltration was compared between genotypes in each area of the spinal cord using non-parametric one-way ANOVA with Bonferroni's multiple comparison test and differences were considered as significant when $P<0.05$.

B.2.4.3. Quantification of axonal loss

Axonal loss was quantified in the spinal cord of MOG-treated animals (see section below) in a minimum of 2 sections per animal in each area of the spinal cord (cervical, thoracic). Coronal spinal cord cryosections immunostained against PLP/NF200 were imaged with a 20x lens and 0.75 digital zoom and further processed and analyzed in ImageJ software, version ImageJA 1.45b (Schneider, et al. 2012). Firstly, images were converted to RGB and then channels were split in black-and-white. A Gaussian filter was applied to enhance signal-to-noise ratio and then a threshold was set to discriminate between postitively stained area and background. This resulted in a binary image (with single objects which were positively stained for NF200) which was analyzed using the particle analysis tool. NF200+ single objects with an area ranging from 0.25 to 1600 µm2 were automatically counted on one hemiside of the spinal cord white matter. Axonal loss was calculated as a percentage in comparison to the axonal density of naïve or CFA-treated mice (previously analyzed in the lab). Data were

expressed as mean±standard error of the mean and statistical analysis was performed using the the GraphPad Prism version 5.00 for Windows (GraphPad Software, San Diego, CA). Axonal loss was compared between genotypes in each area of the spinal cord using non-parametric one-way ANOVA with Bonferroni's multiple comparison test and differences were considered as significant when $P<0.05$.

B.2.5. Fluorescence Activated Cells Sorting (FACS)

For assessing the infiltrating cells of the inguinal and cervical lymph nodes as well as the spinal cord in EAE-induced mice, we performed FACS after isolation of total mononuclear cells and immunostaining against markers of specific types of immune cells. The procedure is explained in detail below.

Isolation of mononuclear cells from spinal cord, cervical and inguinal lymph nodes

Induced mice received an intra-peritoneal injection of anesthesia (per g of body weight: 400 µg of ketamine and 60 µg of xylazine diluted in sterile dH2O in a final volume of 20 µL). Responsiveness to painful stimuli was checked by pinching of the tail or hind limb and we then proceeded to mononuclear cell isolation as follows:

1. Animals were perfused with ice-cold 1xPBS as described above (see section A.I.) in order to remove circulating blood and immune cells.
2. Cervical and inguinal lymph nodes were dissected and the dissection of spinal cords followed. The tissues were cut using a clean razor blade and kept in 1xPBS. Grouped tissues from 1-3 animals of the same genotype were pooled together.
3. Mechanical homogenization of spinal cords in 7 mL 1xPBS and cell isolation from the rest of the tissue by means of a 70 µm cell strainer (#352350, Falcon®).
4. The lymph nodes are centrifuged at 250-300G and staining buffer (5%FBS in PBS) is added and kept at 4^{o}C until further processing (step 7)
5. Addition of 3mL of 30% isotonic Percoll® pH 8.5-9.5 (Mg2+ and Ca2+ free, Sigma-Aldrich) in the cell suspension of the spinal cord tissues and gentle mixing in RT.
6. Mononuclear cells from the spinal cord were isolated using a Percoll® gradient as follows:

- Slow stacking of the cell-containing Percoll mixture on top of 2 mL 70% Percoll® pH 8.5-9.5 (RT).
- Centrifugation at 500 G, 18°C, 30 min, without brakes.
- Careful transfer of 3-5 mL of the intermediate phase in a new tube.
- Washing with a minimum of 8 mL 1xPBS and centrifugation at 500 G, 18°C, 7 min.

1. Resuspension of pellet in 500-1000 µL Staining Buffer (5% fetal bovine serum-FBS in 1xPBS), counting of cells and proceeding to fluorescent staining.

Fluorescent staining of isolated cells and sample analysis

Cells were stained with fluorescence-conjugated antibodies against extracellular markers for 20-30 min, 4°C in Staining Buffer while for intracellular markers (i.e. FoxP3) staining was performed according to manufacturer's instructions (eBioscience) after the extracellular staining. Acquisition was performed using a cell-sorting unit consisting of the DakoCytomation MoFloT High-Performance Cell Sorter (Beckman Coulter, Inc.) and the SummitT software.

B3. Lists of the antibodies used in this study

The antibodies that were used for the immunohistochemistry experiments are described in **Table 4**:

Primary antibody/Epitope	**Source**	**Type**	**Directed against (species)**	**Working dilution**
α-MBP	Serotec	Rat, monoclonal	Human, mouse, rat	1:200
α-PLP (ab28488)	Abcam	Rabbit, polyclonal	Mouse, rat	1:1000
α-NF200	Abcam	Chicken, polyclonal	Human, mouse, rat, chicken	1:15000
α-IBA1	Biocare medical	Rabbit, polyclonal		1:500
4d7 (α-TAG-1)	Developmental Studies Hybridoma Bank	Mouse IgM, monoclonal		1:50
α-NFC1 (pan-Neurofascin)	gift from Dr Peter Brophy, Centre for Neuroregeneration, Chancellor's Building, University of Edinburgh	Rabbit, polyclonal	Human, mouse, rat	1:4000
2ndary abntibody/Epitope	**Source**	**Working dilution**		
α-rabbit IgG-Cy3®	Jackson ImmunoResearch Laboratories	1:800		
α-chicken IgG-FITC	Biotium	1:800		
α-rat IgG- Alexa Fluor® 488	Molecular Probes, Thermo	1:800		
a-mouse IgM 488		1:800		

The antibodies that were used for co-immunoprecipitation experiments were as described in **Table 5**:

Antibody/Epitope	**Source**	**Type**	**Directed against (species)**	**Working dilution**
α-TAG-1, clone 1c12	Developmental Studies Hybridoma Bank	Mouse, monoclonal	Human, rat	1ul/ IP
α-Caspr2	Dr L. Goutebroze, Inserm UMR-S 839, Institut du Fer à Moulin, France	Rabbit, polyclonal	Human, mouse, rat	4ul/IP
α-GFP		Rabbit, polyclonal		4ul/IP

The antibodies that were used for Western Blot experiments were as described in **Table 6:**

Primary antibody/Epitope	**Source**	**Type**	**Directed against (species)**	**Working dilution**
TG2 (α-TAG-1)	Traka et al., 2002	Rabbit, polyclonal	Human, mouse, rat	1:4000
α-Caspr2	Dr L. Goutebroze, Inserm UMR-S 839, Institut du Fer à Moulin, France	Rabbit, polyclonal	Human, mouse, rat	1: 3000
α-GFP		Rabbit, polyclonal		1:10000
α-NFC1 (pan-Neurofascin)	gift from Dr Peter Brophy, Centre for Neuroregeneration, Chancellor's Building, University of Edinburgh	Rabbit, polyclonal	Human, mouse, rat	1:1500
α-c-Myc (A-14)	Santa Cruz Biotechnology, sc-789	Rabbit, polyclonal		1: 1000
2ndary antibody/Epitope	**Source**	**Directed against (species)**	**Working dilution**	
Goat a-rabbit HRPconjugated	Boehringer Mannheim Biochemicals	Rabbit IgG (H+L)	1:5000	

The fluorescent-conjugated antibodies used in FACS were as described in **Table 7**:

Antibody/Epitope	**Source- Cat. No**	**Working dilution**
α-CD4-APC (clone RM4-5)	BioLegend – 100516	1:200
α-CD8-PerCP (clone 53-67)	BioLegend – 100732	1:200
α-CD25-FITC (clone PC61)	BioLegend – 101907	1:200
α-FoxP3-PE	eBioscience (Affymetrix) – 12-5773	1:100

C. Results

C.1. Analysis of the molecular interactions between TAG-1 and Caspr2 and characterization of the specific regions implicated

As already discussed in the introduction, the current hypotheses concerning the interaction of TAG-1 and Caspr2 at the juxtaparanodal region are that: 1) there is an homophilic interaction between glial TAG-1 with the axonal TAG-1 (*in trans*) through their FNIII domains (Tsiotra et al., 1996), 2) there is an heterophilic interaction between axonal TAG-1 and Caspr2 (*in cis*) through the Ig-like subdomains of TAG-1, while the FNIII subdomains do not take place in this interaction (Tzimourakas et al., 2007), 3) in the case of the absence of the axonal TAG-1, the glial TAG-1 physically interacts with Caspr2 and is sufficient for the formation of the Juxtaparanodal complex (Savvaki et al., 2010) and finally 4) in the case of complete absence of either TAG-1 or Caspr2 the result is the disruption of the juxtaparanodal complex and subsequent diffusion of the VGKCs towards the internode (Poliak et al., 2003; Traka et al., 2003; Savvaki et al., 2008). Thus, in the first part of our study we tried to determine which of the Ig-like domains of TAG-1 are responsible for its heterophilic interaction with Caspr2.

For this purpose, we produced six different GFP-tagged deletion plasmid constructs containing different combination of the TAG-1 Ig-like domains and FNIII repeats. These constructs are presented in Figure 12 and all of them are GFP-tagged (N-terminal) and contain a GPI sequence at their C-terminal.

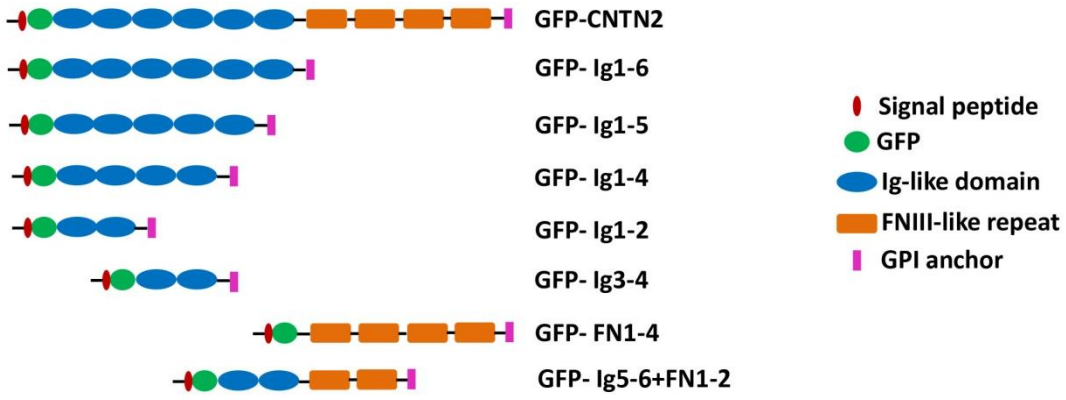

Figure 12: hTAG-1/CNTN2 GFP-tagged deletion constructs produced for identifying the specific TAG-1 subdomains that are implicated in TAG-1 / Caspr2 interaction

Confirmation of the chimeric expression of GFP and the TAG-1 subdomains as well as their localization at the cell membrane (due to the GPI), followed through live immunocytochemistry after transfection of HEK cells (Figure 13).

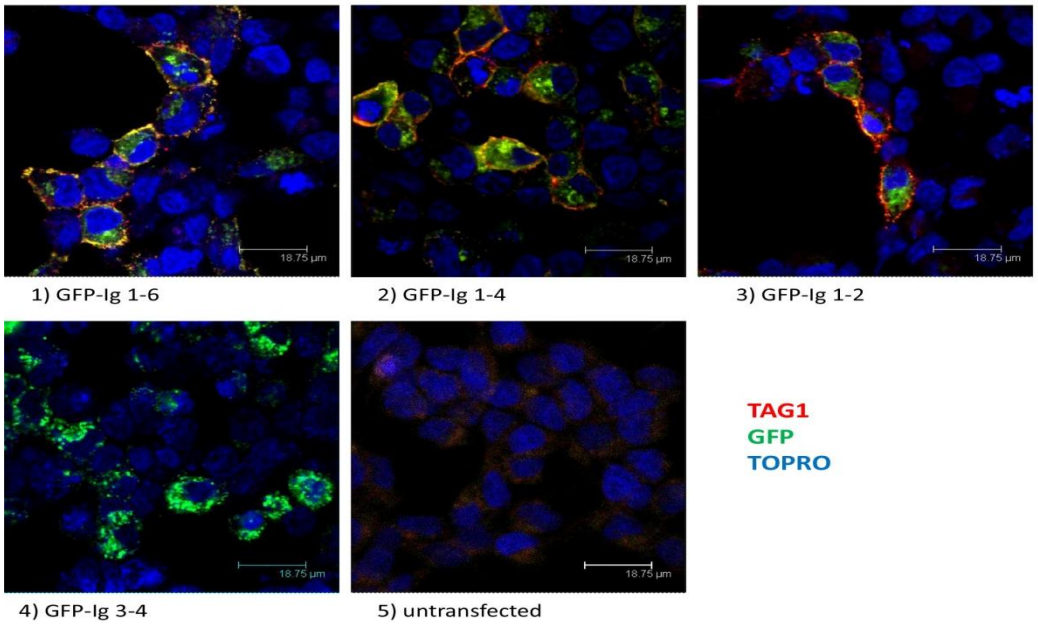

Figure 13. Expression of the hTAG-1/CNTN2 deletion constructs after transfection of HEK293T cells and immunocytochemistry on live cells.

After validating the expected molecular weight of each deletion construct through Western blot (Fakoureli Eirini's Diploma thesis, 2014), we continued with co-transfection of HEK293T cells with one hTAG-1 deletion construct each time, combined with a construct expressing hCaspr2 (#330). Then Co-immunoprecipitation experiments took place, using an anti-TAG-1 (or anti-GFP) antibody and examination through WB analysis of whether Caspr2 was precipitated together with each TAG-1 subdomain, followed.

The molecular weight (MW) of hCaspr2 is ~150kDa, while the expected (MW) of each TAG-1 subdomain are presented in **table 8**:

hTAX-1 subdomain	**Molecular Weight**
(hTAX-1) +GFP	~150kDa
(FN1-4+GPI)+ GFP	~97.2kDa
(Ig1-6+GPI)+GFP	~91.6kDa
(Ig1-5+GPI)+GFP	~82.4kDa
(Ig1-4+GPI)+GFP	~70.9kDa
(Ig1-2+GPI)+GFP	~49.67kDa
(Ig3-4+GPI)+GFP	~46.93kDa
(Ig5-6,FN1,2+GPI)+GFP	~80.18kDa

Firstly we confirmed that the total hTAG-1 protein as well as the Ig1-6 subdomains of TAG-1, interact directly with Caspr2 as previously shown (Tzimourakas et al., 2007) (Figure 14).

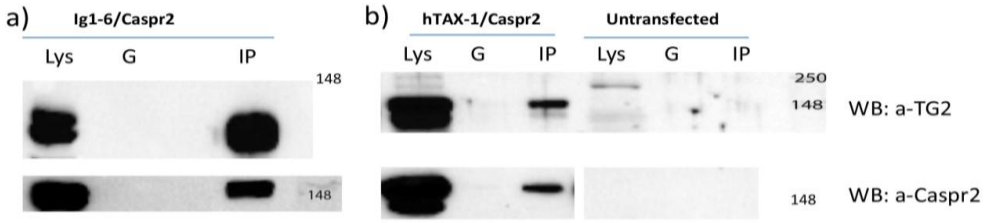

Figure 14. Co-immunoprecipitation analysis of HEK293 co-transfected cells: direct interaction of a) Ig1-6 subdomains of hTAG-1 with hCapsr2 and b) of total hTAG-1 with hCapsr2 (left), untransfected cell lysate was used as negative control (right). Immunoprecipitation with anti-TAG-1 antibody 1c12; WB: Western blot analysis of the lysates (Lys), G-beads (G) and Immunoprecipitates (IP)

We continued with examining the possible interaction of the rest of the TAG-1 subdomains with Caspr2. As the subdomain constructs are fused with GFP, we conducted IP using an α-GFP antibody. Surprisingly, an interaction could be detected between hTAX-1 subdomains Ig1-2, Ig1-4, Ig3-4 and Caspr2 (Figure 15a and 16), but no clear interaction could be observed between Ig1-5 and Caspr2 (Figure 16). Another surprising observation was that we could detect a direct interaction between the FNIII-repeats of hTAG-1 and Capsr2 (Figure 15b), something that is opposite to what has been observed in Tzimouraka's et al., 2007. Last but not least, the Ig5-6+FN1-2 subdomain of hTAG-1 could also interact with Caspr2 (Figure 15b).

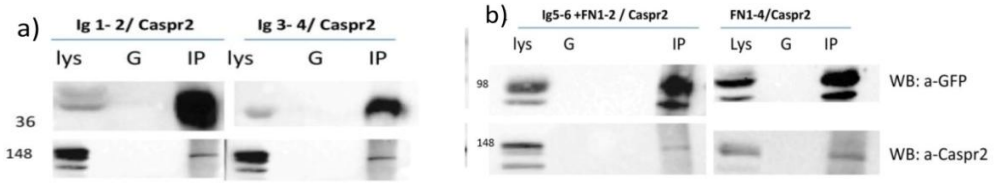

Figure 15. Co-immunoprecipitation analysis of HEK293 co-transfected cells: direct interaction of **a)** Ig1-2(left) and Ig3-4(right) subdomains of hTAX-1 with hCaspr2 and of **b)** Ig5-6+FN1-2(left) and FN1-4 (right) subdomains of hTAX-1 with hCaspr2. Immunoprecipitation with α-GFP antibody; WB: Western blot analysis of the lysates (Lys), G-beads (G) and Immunoprecipitates (IP)

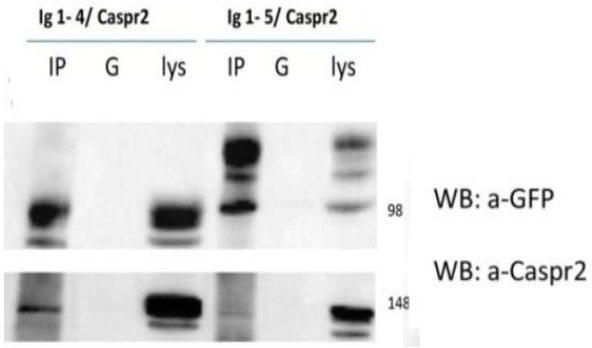

Figure 16. Co-immunoprecipitation analysis of HEK293 co-transfected cells: a direct interaction is observed between Ig1-4subdomain of hTAX-1 and hCaspr2 (left), while no clear interaction can be observed between Ig1-5 subdomains of hTAX-1 and hCaspr2 (right). Immunoprecipitation with anti-GFP antibody; WB: Western blot analysis of the lysates (Lys), G-beads (G) and Immunoprecipitates (IP)

In order to confirm our results, we conducted the exact same procedure with the difference that in this case, we used an anti-Caspr2 antibody during the co-IP experiments. Thus, we examined whether each of the hTAG-1 subdomains could be precipitated together with hCapsr2, meaning that they can directly interact. The results confirmed our previous observations, as the only case in which we could not detect an interaction with Caspr2 concerned the Ig1-5 sudomains (Figure 17). For negative controls, we used lysates from

untransfected HEK293T cells and from transfected cells with a plasmid construct expressing only Caspr2 (mentioned as “Caspr2” on figure 17) HEK293T cells.

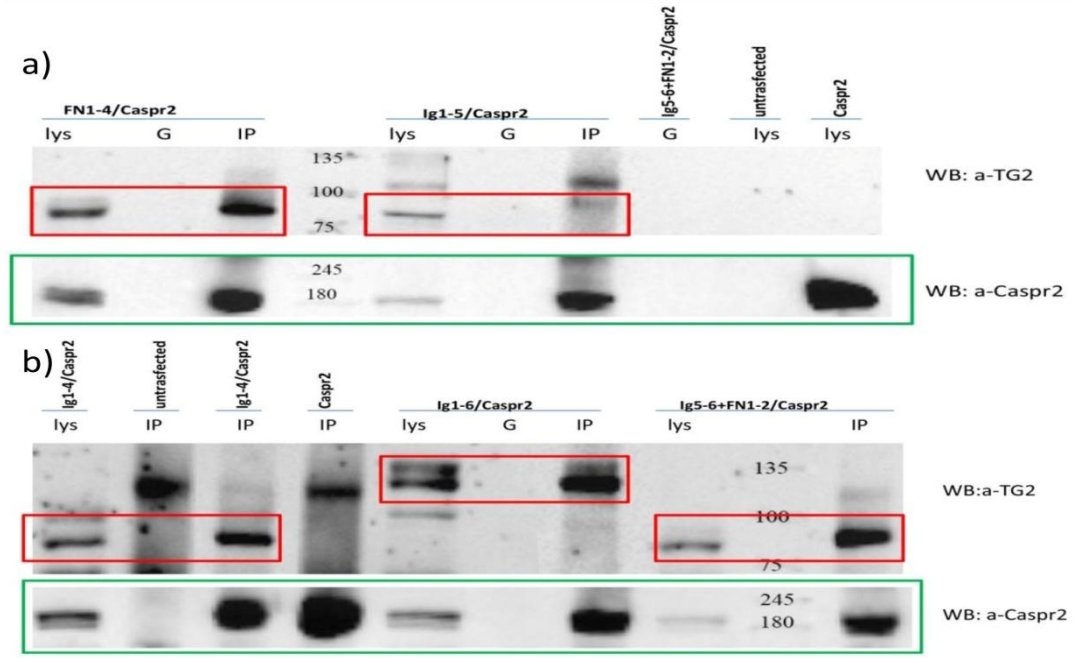

Figure 17. Confirmation of the results observed in figures 14-16, after Co-immunoprecipitation analysis of HEK293 co-transfected cells using an anti-Caspr2 antibody: a) a direct interaction is observed between FN1-4 and Caspr2 (left), while no clear interaction can be observed between Ig1-5 and Caspr2 (middle) b) direct interaction is observed between Ig1-4 (left), Ig1-6 (middle) and Ig5-6+FN1-2 (right). Untransfected and transfected with a plasmid construct expressing only Caspr2 (mentioned as “Caspr2”) HEK293T lysates were used as negative controls. Immunoprecipitation with anti-Caspr2 antibody, WB: Western blot analysis of the lysates (Lys), G-beads (G) and Immunoprecipitates (IP)

C.1.2. Examination of the role of secreted TAG-1 in the TAG-1/Caspr2 interaction

In the publication of Savvaki et al., 2010, it was shown that glial TAG-1 can interact with Caspr2 in the absence of axonal TAG-1. Moreover, for the first time the *trans* interaction of glial TAG-1 and Caspr2 was mentioned, without excluding the possibility that the secreted form of TAG-1 might play a role in this interaction and thus in the formation of the juxtaparanodal complex (see Discussion). Thus, we tried to examine whether the addition of a secreted form of TAG-1 (coming from a cell culture of Lepidoptera that expresses it stably, see materials & methods) on the supernatant medium of the co-transfected HEK293T cells, could affect the interactions.

More specifically, we first tested the possible effect of the released form of TAG-1 in the interaction between the total hTAX-1 protein and hCaspr2 (figure 18). In this case we could not observe any significant difference in the signal of the co-immunoprecipitated Caspr2 after the addition of the released form of TAG-1.

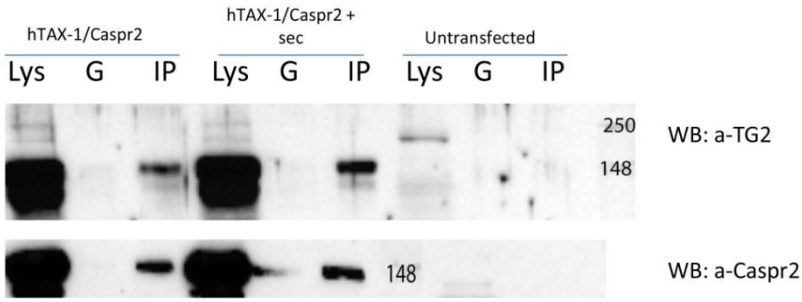

Figure 18. Effect of a released form of TAG-1 in the hTAX-1/Caspr2 interaction: Co-immunoprecipitation analysis of HEK293 co-transfected cells with(middle) and without (left) addition of a released form of TAG-1: No significant difference can be observed between the two cases. Untransfected cell lysate in which secreted TAG-1 was added, was used as negative control (right). Immunoprecipitation with anti-TAG-1 antibody 1c12; WB: Western blot analysis of the lysates (Lys), G-beads (G) and Immunoprecipitates (IP)

Our next step was to examine the possible effect of the secreted form of TAG-1 between the interaction of the Ig1-6 subdomains or the FN1-4 subdomains of hTAX-1 and hCaspr2. Interestingly, the signal of Caspr2 that was precipitated together with the TAG-1 subdomains was less intense in both cases (figure 19).

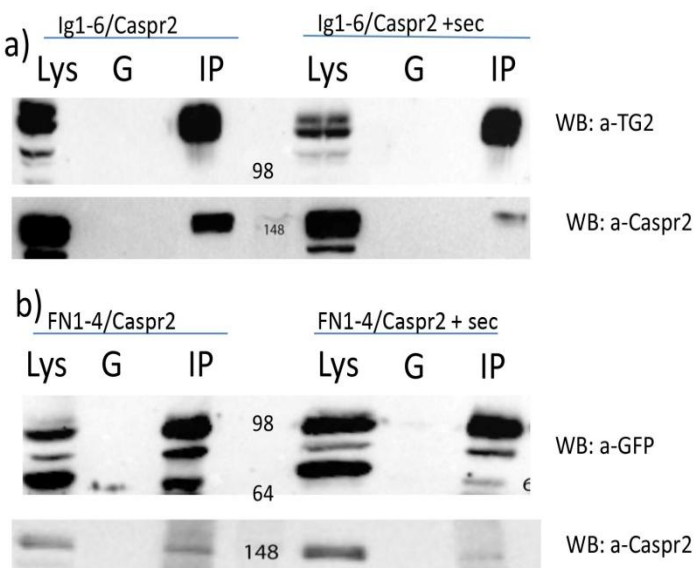

Figure 19. Effect of a released form of TAG-1 in the interaction between the Ig subdomains (a) or the FNIII subdomains (b) of hTAG-1 and hCaspr2: Co-immunoprecipitation analysis of HEK293 co-transfected cells with(right) and without (left) addition of secreted TAG-1: A decrease in the signal of the co-precipitated Caspr2 is observed after the addition of the secreted form of TAG-1 in both cases. Immunoprecipitation with anti-TAG-1;1c12 (a) or anti-GFP(b) antibody; WB: Western blot analysis of the lysates (Lys), G-beads (G) and Immunoprecipitates (IP)

C.2. TAG-1 direct interaction with Sema6A, NF140 and NF155

In this part of our study, we used UniReD (created by Dr I. Iliopoulos lab, Medical School, University of Crete), a computational tool that takes advantage of Biomedical literature in order to extract not only known protein-protein interactions, but also undocumented ones. UniReD revealed a number of known protein interactors for the target molecule TAG-1/CNTN2 (CNTN2, UniProt ID:Q61330, as well as several other potent interactors. We thus tried to validate some of the UniReD results, concerning the putative interactors,

experimentally. Two of the potent interactors that UniReD suggested were Sema6A (UniProt ID:O35464) and Neurofascin (NFASC, UniProt ID:Q810U3) (figure 20).

UniRed results for query protein Q61330 and mcl inflation value 3

Cluster Score	UniProt ID	Protein Name
	Q61330	CNTN2_MOUSE
0.342911489213	O35464	SEM6A_MOUSE
0.384952668058	Q810U3	NFASC_MOUSE

Figure 20. UniReD cluster scores of the potent interactors of TAG-1: Sema6A and NFASC

The experimental approach we followed in order to validate the results of UniReD, included co-transfection of HEK293 cells with a construct expressing GFP-tagged hTAG-1 (#621) and either a Sema6A, a NF140 or a NF155 expressing plasmid construct followed by co-IPs using an anti-TAG-1 antibody. We indeed observed and interaction in all cases after Western blot analysis (Figure 21).

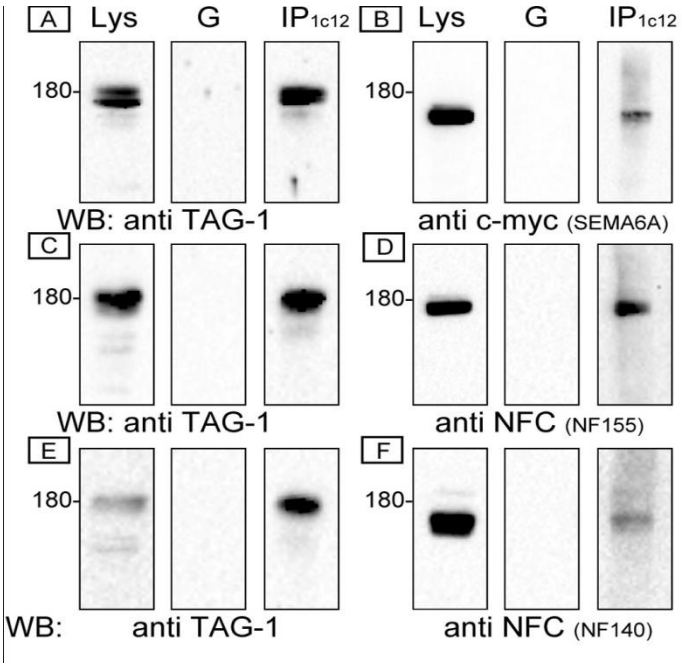

Figure 21. Co-immunoprecipitation analysis of HEK293 co-transfected cells. **A-F.** Direct interactions of TAG-1 with Sema6A (**A,B**), Neurofascin155 (NF155) (**C,D**) and Neurofascin140 (NF140) (**E,F**) in HEK293 co-transfected cells. Immunoprecipitation was performed with the monoclonal anti TAG-1 antibody 1c12. Western blot analysis of the lysates (Lys), G-beads used for the preclearance step (G) and Immunoprecipitates (IP_{1c12}) revealed the direct interaction of GFP-tagged TAG-1 with Sema6A-c-myc (**B**), NF155 (**D**) and NF140 (**F**)

In order to further validate our results, we conducted an immunohistochemistry experiment, where we examined whether we could detect a co-localization of TAG-1 and Neurofascin in the brain of wild type mouse embryos at embryonic day 13,5 (E13,5). At E13,5 both NF140 and NF155 have been reported to be expressed mouse hind brain (Zhang et al., 2015). We could see co-localization of TAG-1 and Neurofascin in specific regions of the forebrain, the midbrain and the hindbrain (figure 22).

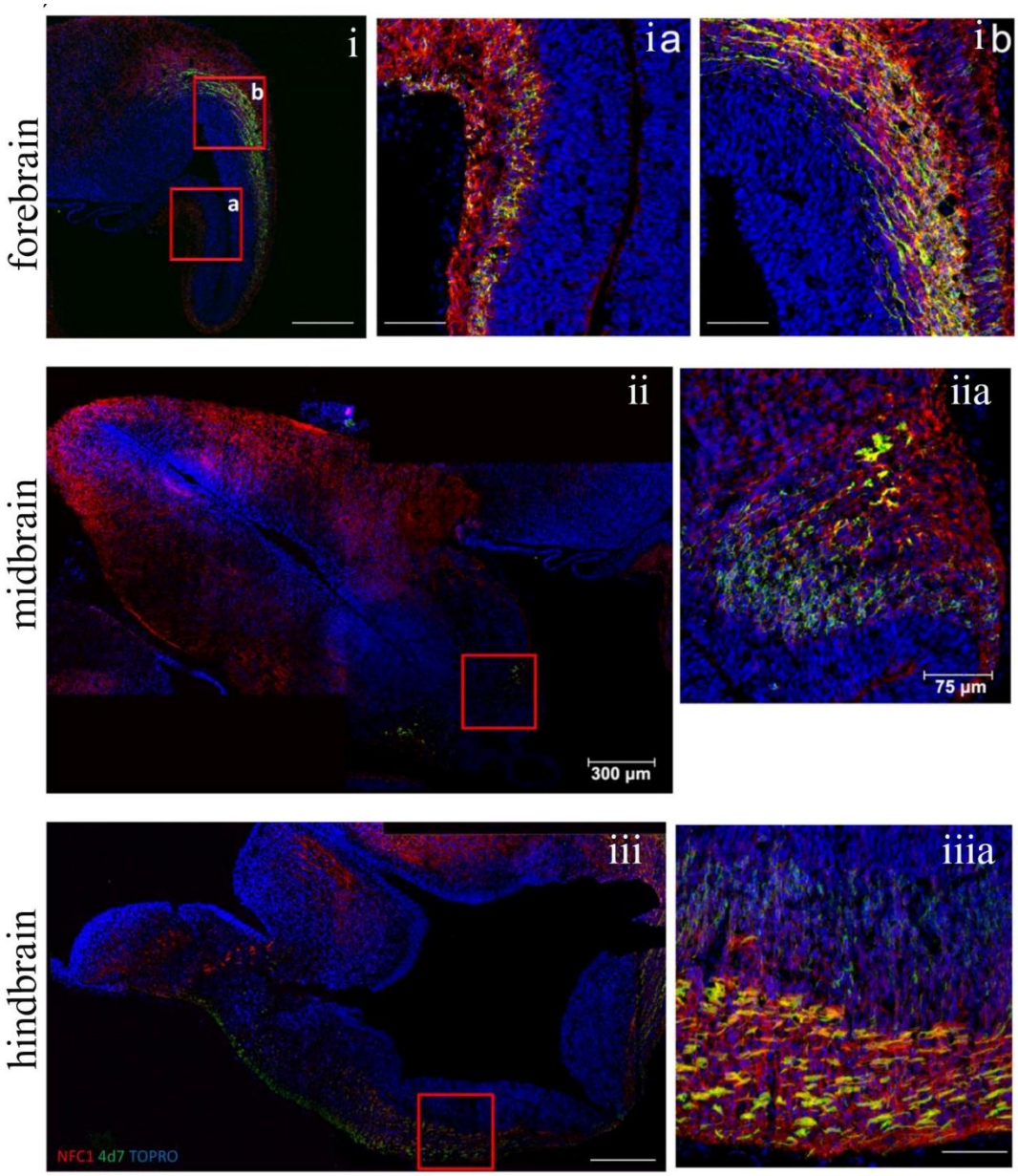

Figure 22. TAG-1 and Neurofascin co localization in E13,5 mouse forebrain (i), midbrain (ii) and hind brain (iii). In figures I,ii,iii the scale bar corresponds to 300µm, while in figures ia,ib,iia,iiia the scale bar corresponds to 75µm. The red boxes in figures I,ii,iii correspond to zoom areas that are presented in ia,b, iia and iiia respectively. TAG-1: 4d7 antibody (green);Neurofascin: pan NFC1 antibody (red); the cell nuclei are stained with TOPRO. The yellow signal verifies co-localization.

C.3. EAE induction on *Tag-1+/+* versus *Tag-1-/-* mice

EAE induction was performed on C57BL/6 female mice. This strain shows the appropriate responsiveness as it bears the major histocompatibility locus H-2 (MHC_{H-2}) shown to be indispensable for disease onset (Montgomery and Rauch, 1982). *Tag-1-/-* and *Tag-1 +/+* were introduced in the C57BL/6 background previously in the lab (Kastriti's M. PhD thesis). The juxtaparanodal phenotype of *Tag-1-/-* mice of this background was examined and diffusion of Caspr2 and VGKCs was detected, similarly to the already described ohenotype in

the C57B110/CBA background (Savvaki et al., 2008). Moreover, the stages, clinical signs and the most well established histopathological findings (e.g. infiltration, axonal loss and demyelination) of MOG_{35-55}-induced EAE on this background has been analyzed in our lab.

Briefly, the induced disease was characterized by discrete stages of symptom severity, while the control group that received only CFA did not exhibit any of the symptoms (Figure 23). Initially, the first days post-induction (dpi) are symptom-free, and an initial onset is observed around 10-11dpi. In a matter of 3-5days the clinical score reaches a maximum, which last for 2-4 days, followed by partial recovery. Almost a week later, mice show the first relapsing-remitting episode and relapses from then on are characterized by reduced symptom severity overtime (Figure 23).

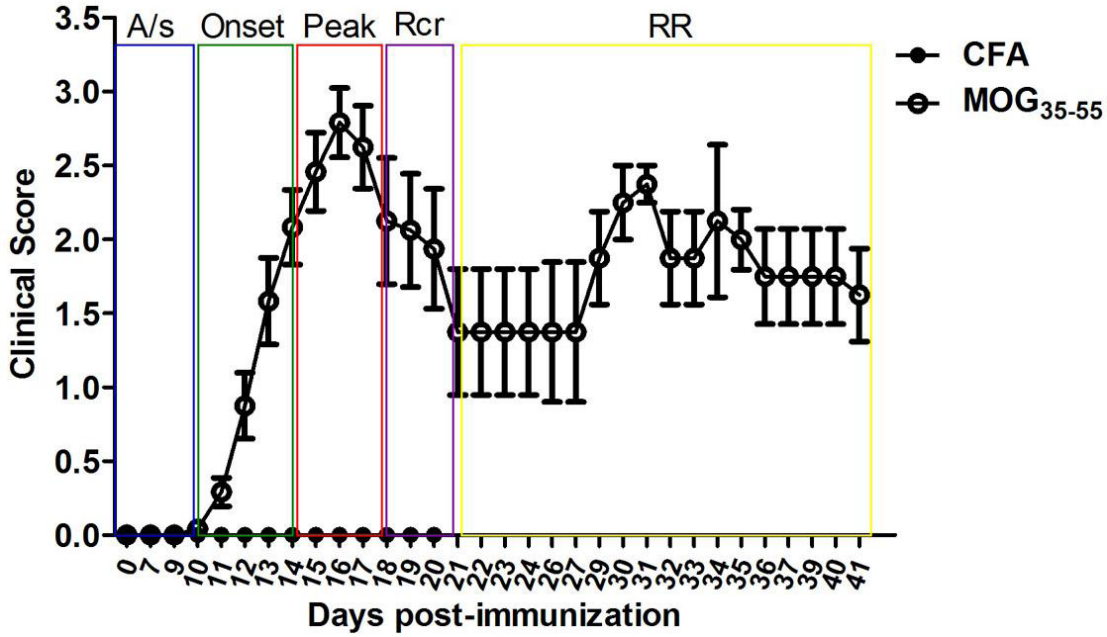

Figure 23: Clinical course of EAE in the C57BL/6 background. The diagram depicts the discrete stages of the acute disease followed by a relapsing-remitting stage assessed by daily scoring (MOG_{35-55}) versus the control CFA group, in which no symptoms were observed. Scale of clinical symptoms: 0: no neurological signs; 1:flaccid tail; 2: hindlimb (HL) weakness or abnormal gait; 3: complete HL paralysis; 4: complete HL paralysis and weakness of the forelimbs. CFA: Complete Freund;s Adjuvant; A/s: assymptomatic; Rcr: recovery; RR: Relapsing-Remmiting. (Kastriti's PhD thesis)

Based on the clinical course described above, the degree of spinal cord infiltration, white matter (WM) demyelination and axonal loss was analyzed at the following time points: 16dpi, corresponding to the peak of the disease, 20dpi, where recovery has already initiated and 40dpi, when the pathology is considered to be chronic.

Briefly, following EAE induction in WT mice, at 16dpi migroglial/macrophage infiltration is of the same degree both in the WM and GM, demyelination is more profound compared to later stages and axonal degeneration has already initiated. At 20dpi, infiltrates are mostly found at WM areas and a significant degree of demyelination in all areas accompanied by axonal loss ranging from 20-40% (reduced compared to 16dpi especially in cervical and thoracic areas) could be observed. At 40dpi, migroglial/macrophage infiltration is greatly

reduced. At the same time, cells of immune identity are populating areas of former lesions and there is a significant degree of axonal recovery. (Kastriti's M. PhD thesis)

Our next step, mainly undertaken by this study, was the analysis of susceptibility, disease course and duration in the absence of TAG-1. Taking into account the implication of TAG-1 in MS pathology as a potential autoantigen (Derfuss et al., 2009), we tried to test the hypothesis that in its absence demyelination or remyelination might be affected. We chose to induce EAE to wild type and *Tag-1-/-* mice at 20dpi (substantial inflammation, demyelination and axonal loss) and 40dpi and analyze comparatively their clinical picture and pathology. Firstly, the analysis of 20dpi took place and then a similar analysis followed at 40dpi.

Initially, following induction, both genotypes presented symptoms on the same days (Figure 24), but mutant mice showed significantly reduced symptom severity early after the onset of clinical symptoms. Eventually, both genotypes reached similar maximum scores, but in mice lacking TAG-1 this happened with a delay of 3-5 days compared to WT. This was followed by partial recovery which was less intense in mice lacking *Tag-1-/-*. Intriguingly, the symptom severity was significantly higher at *Tag-1-/-* mice during the RR stage of the disease.

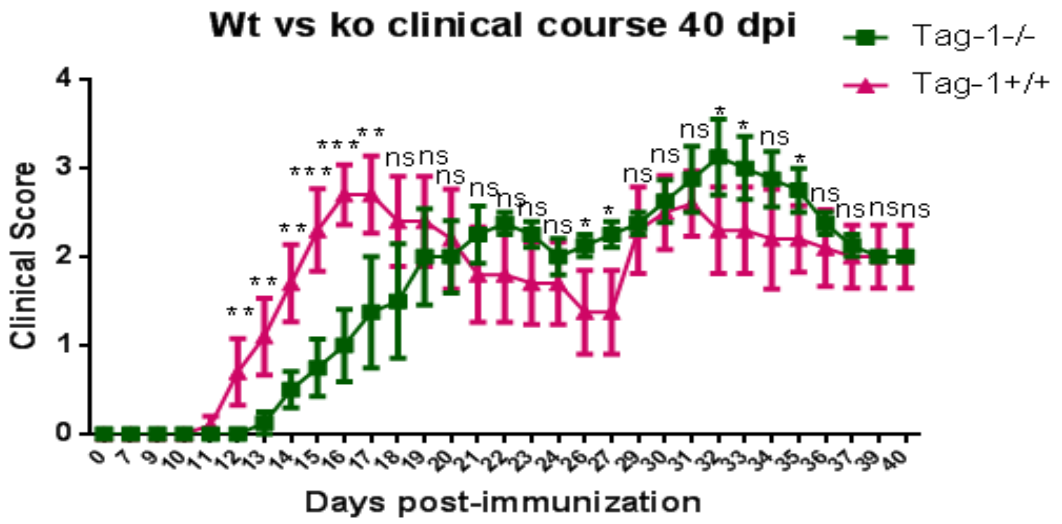

Figure 24: Clinical course and severity of EAE in *Tag-1+/+* and *Tag-1-/-* mice. Graph showing the course of symptoms after daily scoring. N=5 (*Tag-1+/+)* and 4 (*Tag-1-/-).* Scale of clinical symptoms: 0: no neurological signs; 1:flaccid tail; 2: hind limb (HL) weakness or abnormal gait; 3: complete HL paralysis; 4: complete HL paralysis and weakness of the forelimbs. (t test: ns: non-significant; P<0.05: *; P<0.01: **; P<0.0001: ***)

C.3.1. Demyelination degree and axonal loss in *Tag-1+/+* and *Tag-1-/-* mice

Next, we went on to analyze the degree of demyelination and axonal degeneration at acute (20dpi) and chronic (40dpi) stage, in the two genotypes (Figure 25). The analysis took place at the cervical, thoracic and lumbar areas at 20dpi and at the cervical and thoracic areas at 40dpi.

In all of the experiments, spinal cord infiltration by macrophages and microglia was examined through inspection of the ionized calcium-binding adapter molecule 1 (IBA1). The degree of demyelination was analyzed through immunostaining against the myelin protein PLP and axonal loss through immunostaining against the 200kDa Neurofilament protein (NF200) in the different regions of the spinal cord (cervical, thoracic and in some cases lumbar).

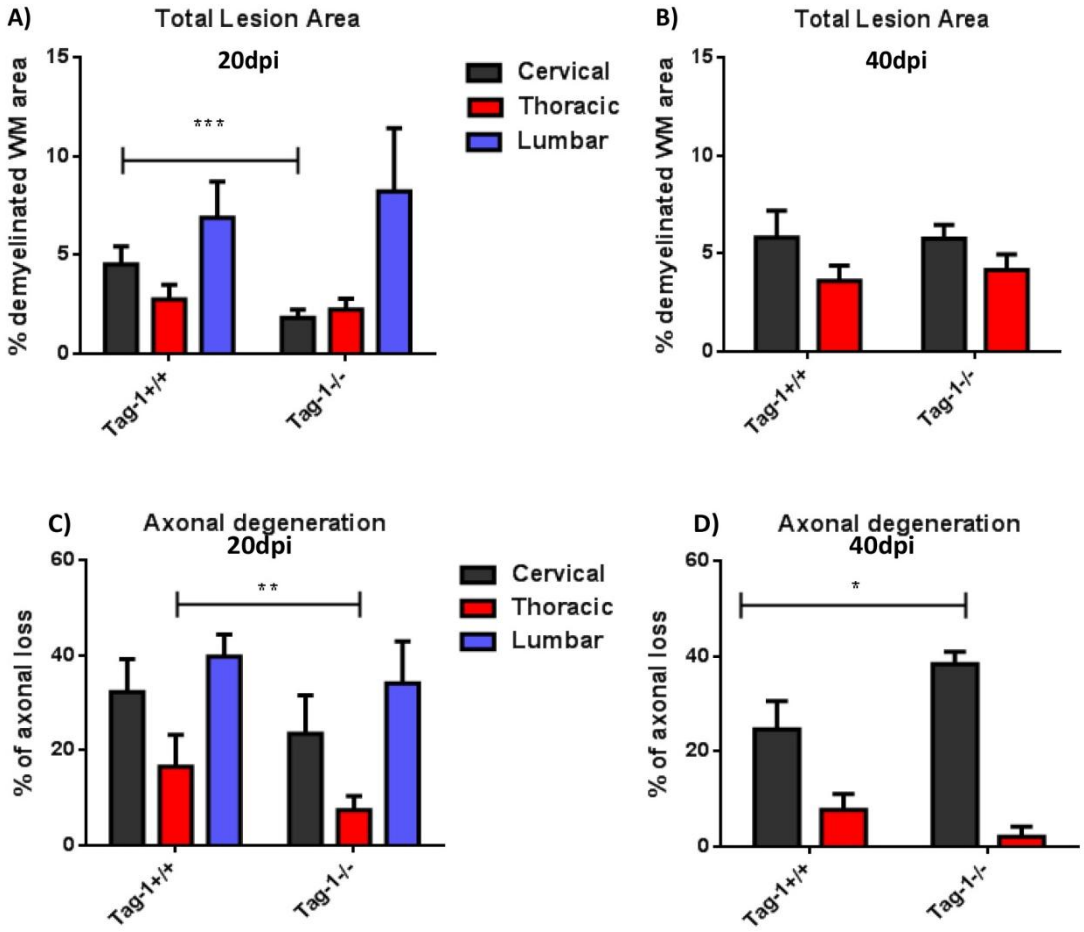

Figure 25: Analysis of demyelination and axonal loss in EAE *Tag-1+/+* versus *Tag-1-/-* mice at 20dpi(A and C) and 40dpi (B and D). A) Graph of the quantified total demyelinated areas of the WM in EAE-induced mice at 20dpi and B) 40dpi, and C) the axonal loss at 20dpi and D) 40dpi, at cervical, thoracic and lumbar areas. At 20dpi: N=6 (*Tag-1+/+)* and 7 (*Tag-1-/-)* and at 40dpi: N=4 (*Tag-1+/+)* and 3 (*Tag-1-/-).* (t test; P<0.05: *; P<0.01: **; P<0.0001: ***)

At 20dpi, in wild type mice, the most prominent demyelination and axonal loss were observed at cervical and lumbar areas, while this holds true only for the lumbar area in the case of mutant mice (Figure 25 A and C). However even in the absence of demyelination, axonal loss in cervical areas is pronounced in both genotypes. Additionally, the thoracic spinal cord, even though is similarly demyelinated in the two genotypes, the extend of its axonal loss in the mutant mice is smaller. We had previously shown that the axonal density does not differ between naïve wild type and mutant mice (Kastriti's M. PhD thesis).

At 40dpi, demyelination between *Tag-1-/-* and *Tag-1+/+* mice did not present any significant difference neither in the cervical nor in the thoracic area (Figur25B). On the other hand, in the cervical area the axonal loss was significantly higher in the mutant mice compared to wild type. More specifically, in wild type, the % axonal loss has been decreased when compared to 20dpi, while in the mutants the % axonal loss remains at similar or even higher levels in the case of the cervical area when compared to 20dpi.

C.3.2. Analysis of the profile of inflammatory infiltrates in the absence of TAG-1

From the analysis of the EAE-induced wild type animals, we observed that IBA1 infiltration levels at 20dpi correlate with total lesion area and axonal loss. Furthermore, at 20dpi there was a preference of IBA1+ for the WM versus the GM of the spinal cord. Based on these observations we wondered whether the same happens in the absence of TAG-1. To address this, we performed quantification of IBA1+ area in total spinal cord sections at WM or GM areas (Figure 26).

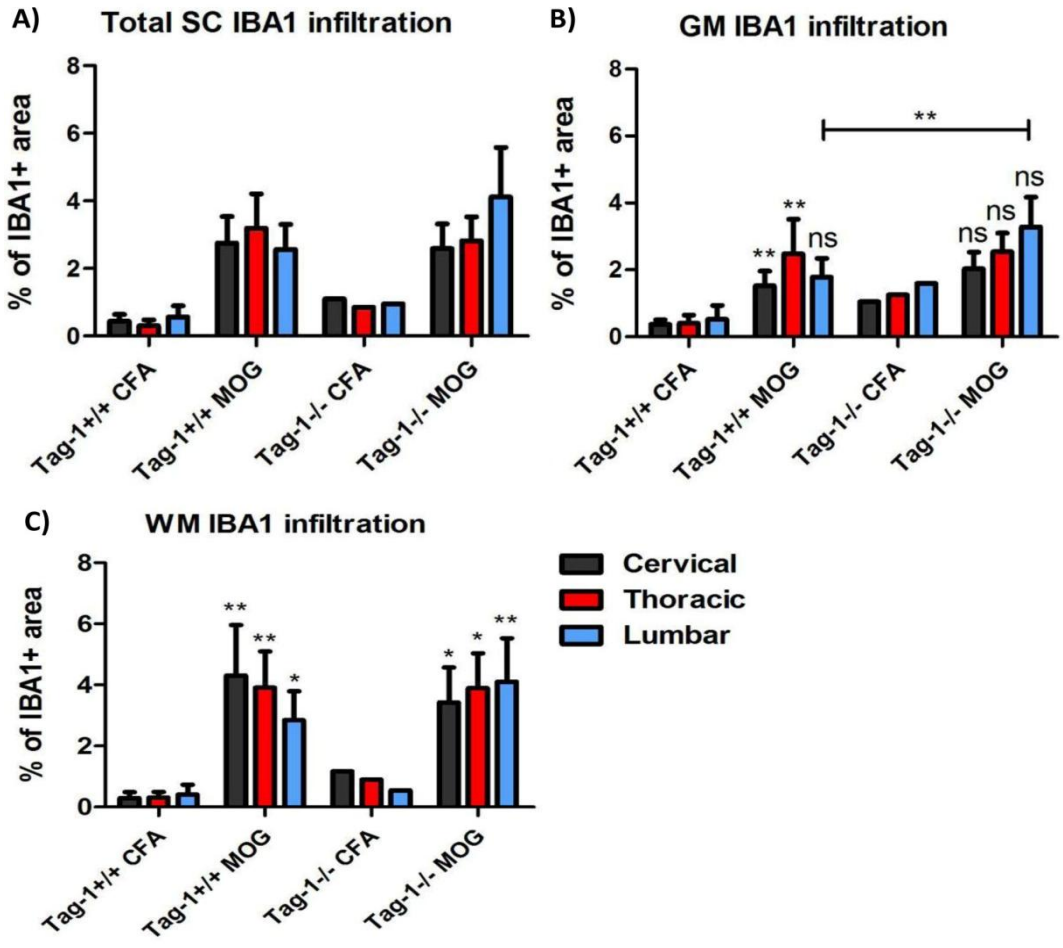

Figure 26. Analysis of IBA1+ infiltrates in the spinal cord of induced *Tag-1+/+* versus *Tag-1-/-* mice at 20dpi. Quantification of A) total spinal cord infiltrates, B) infiltrates at the gray matter of the spinal cord and C) infiltrates at the white matter of the spinal cord. N=6 (*Tag-1+/+)* and 7 (*Tag-1-/-)* (1-way ANOVA; ns: non-significant; P<0.05: *; P<0.01: **)

Inspection of the spinal cord from cervical to lumbar levels revealed that *Tag-1-/-* induced mice show increased IBA1+ signal at the lumbar spinal cord, while in the rest of the spinal

cord infiltration seems comparable (Figure 26A). This seems to correspond mainly to increased levels of WM infiltrates (Figure 26B, C). Interestingly, the majority of microglial cells at the spinal cord of wild type mice are found at the rostral part (cervical and thoracic). On the other hand, in knock-out mice these cells seem to be mostly located at lumbar areas, indicating a possible delay in their progression from the posterior to the anterior spinal cord.

We then tried to examine whether this "delay" in the progression of IBA1+ observed in 20dpi induced knock-out mice, was altered at 40dpi by analyzing the cervical and thoracic areas (Figure 27). The % IBA1+ infiltration was reduced at 40dpi in the total spinal cord (WM+GM) in both cervical and thoracic areas (Figure 27C) when compared to 20dpi (Figure 26A). The WM IBA1 infiltration of MOG-induced animals was significantly higher when compared to CFA only in the case of the cervical area, while there was no significant difference between the two genotypes (Figure 27A). The GM IBA1 infiltration of MOG-induced mice was in both genotypes comparable with that of the CFA group.

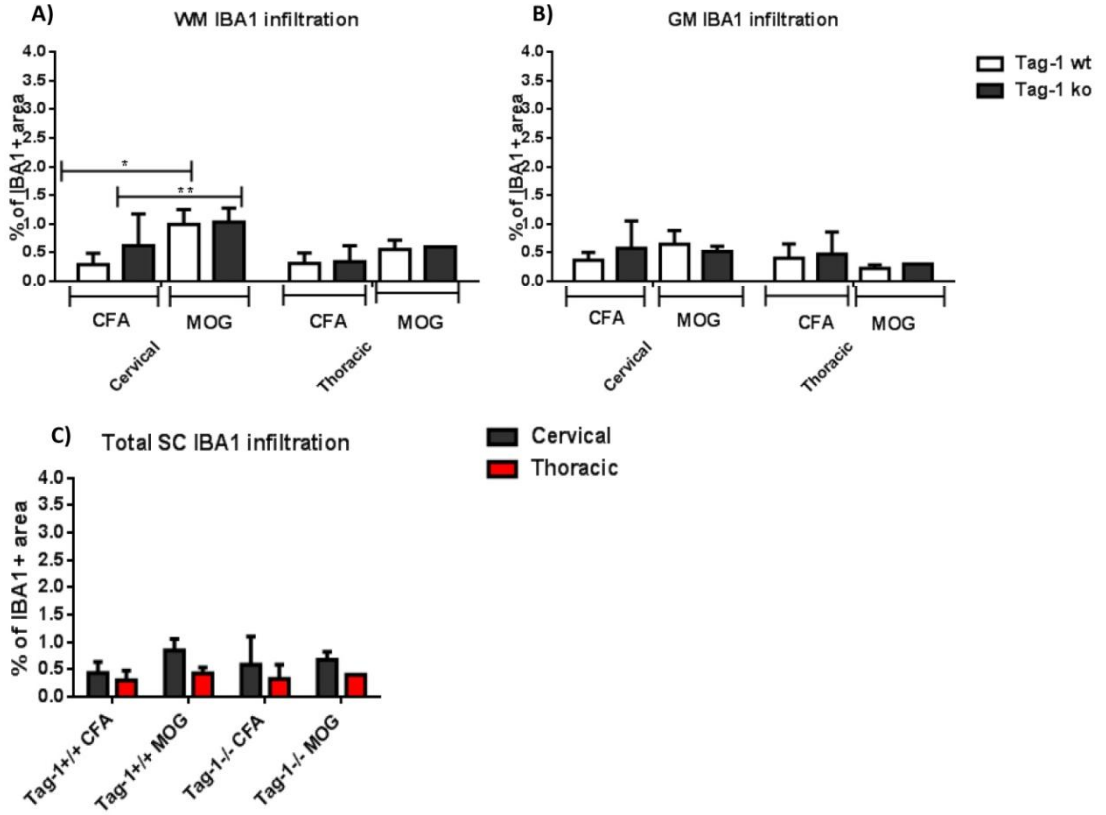

Figure 27: Analysis of IBA1+ infiltrates in the spinal cord of induced *Tag-1+/+* versus *Tag-1-/-* mice at 40dpi. Quantification of A) total spinal cord infiltrates, B) infiltrates at the gray matter of the spinal cord and C) infiltrates at the white matter of the spinal cord. N=4 (*Tag-1+/+)* and 3 for cervical, 1 for thoracic (*Tag-1-/-)* (1-way ANOVA; P<0.05: *; P<0.01: **)

Nevertheless, IBA1+ cells do not account alone for disease onset or propagation in EAE, since other cells of both adaptive and innate immune system take part in this process. We previously attempted to address directly the activation of the immune system. To this end, the total mononuclear cells were isolated from the spinal cords of induced animals. More specifically, this took place at the peak of the disease (16-18dpi) for both genotypes and analyse for markers of T cells and B cells using FACS. This analysis showed that the

percentages of total T cells, B cells as well as the subpopulations of helper and cytotoxic T cells (T_H and T_C respectively) are comparable in the two genotypes. Interestingly though, a significant reduction was observed in the fraction of the regulatory T cells (T_{regs}) in *Tag-1-/-* compared to wild type animals.

In the present study we tried to repeat the FACS experiment in order to confirm the result concerning the reduction of T_{regs} in the spinal cord of mutant mice, while we tried to detect any possible differences concerning this cell population at the lymph nodes of *Tag-1-/-* and *Tag-1+/+* animals. T_{regs} express the biomarkers CD4, Foxp3 and CD25.

Firstly, we were able to reproduce the reduction of the T_{regs} population in the knock-out mice (Figure 28B) when compared to wild type (Figure 28A). More specifically, in Figure 28C, we can see that the WT triple positive cells show a normal distribution concerning the expression of the 3 markers. On the conteary, in the KO triple positive cells we can observe a cell population that presents reduced expression of the Foxp3 marker.

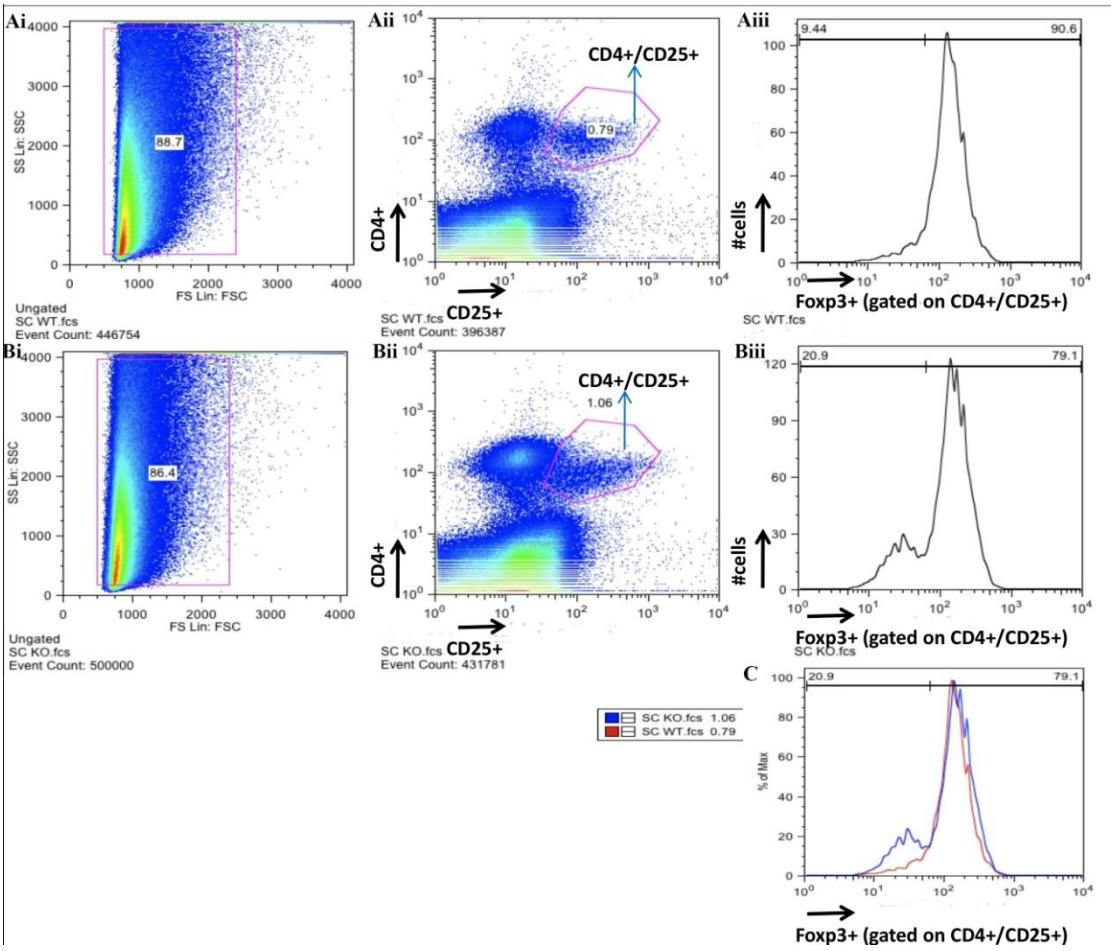

Figure 28: Analysis of CD4+/CD25+/Foxp3+ T_{regs} in the spinal cord (SC) of EAE induced *Tag-1+/+* (A) versus *Tag-1-/-* (B) mice. In Ai and Bi, the SSC (Side Scatter) which shows the cell size, is plotted against the FSC (Forward Scatter) which shows the granulation of the cells. The cells in the purple box were chosen for further analysis. In Aii and Bii, the purple circle corresponds to the double positive CD4+/CD25+ cells that we chose for further analysis. Y and X axis correspond to the expression of CD4+ and CD25+ respectively. In Aiii and Biii, we see the distribution of cells chosen from Aii and Bii that are positive for Foxp3+, so we observe the triple positive CD4+/CD25+/Foxp3+ cells. In C we see a

comparison between the triple positive cell distribution of the wild type (WT: red) versus the knock-out (KO: blue) induced mice.

Furthermore, we performed a similar analysis of the T_{regs} at the inguinal lymph nodes (Ing LN) of the knock out (Figure 29B) versus the wild type (Figure 29A) EAE-induced mice. We saw that in the Ing LN of *Tag-1+/+* EAE-induced mice the triple positive CD4+/CD25+/Foxp3+ T_{regs} were reduced when compared to *Tag-1-/-* EAE-induced mice (Figure 29C).

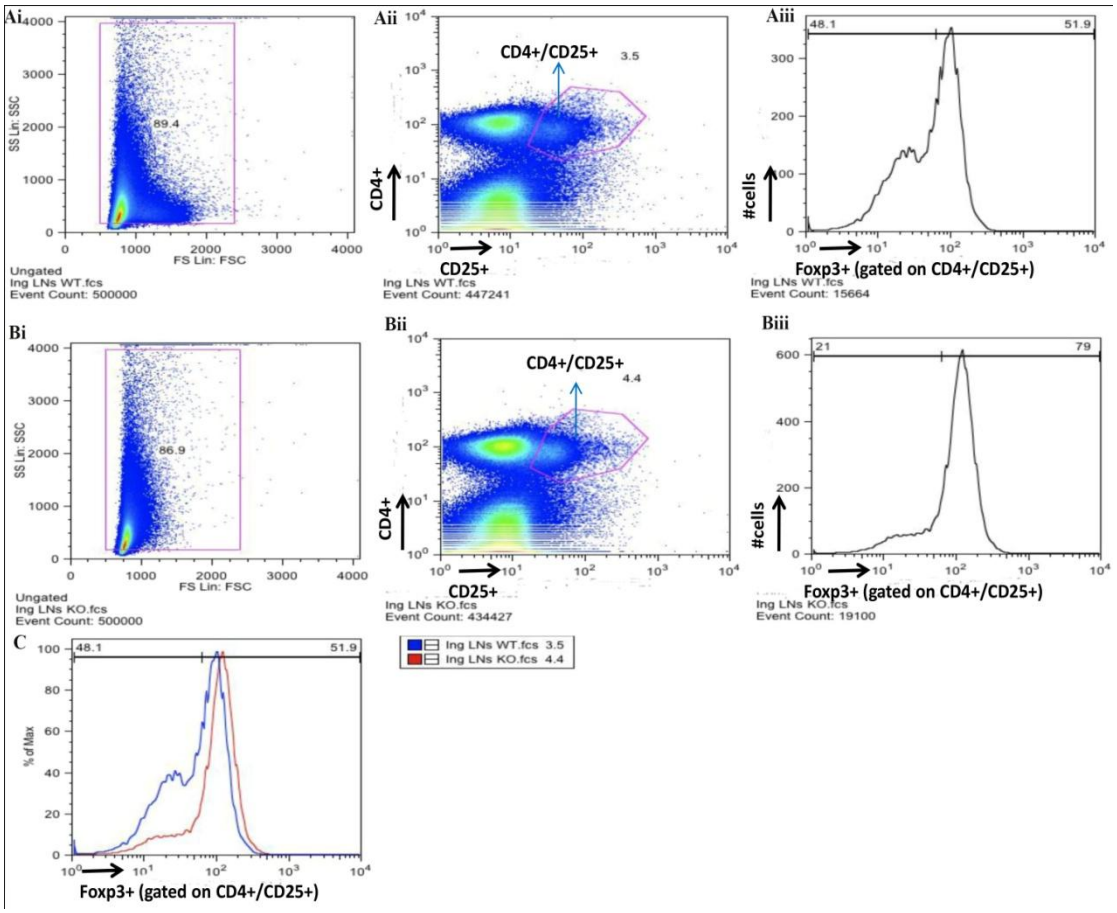

Figure 29: Analysis of CD4+/CD25+/Foxp3+ T_{regs} in the inguinal lymph nodes (Ing LN) of EAE induced *Tag-1+/+* (A) versus *Tag-1-/-* (B) mice. In Ai and Bi, the SSC (Side Scatter) is plotted against the FSC (Forward Scatter). The cells in the purple box were chosen for further analysis. In Aii and Bii, the purple circle corresponds to the double positive CD4+/CD25+ cells that we chose for further analysis. Y and x axis correspond to increased expression of CD4+ and CD25+ marker respectively. In Aiii and Biii, we see the distribution of cells chosen from Aii and Bii that are positive for Foxp3+, so we observe the triple positive CD4+/CD25+/Foxp3+ cells. In C we see a comparison between the triple positive cell distribution of the wild type (WT: blue) versus the knock-out (KO: red) induced mice.

A similar observation took place when we compared the triple positive CD4+/CD25+/Foxp3+ T_{regs} of the cervical lymph nodes of wild type and knock-out animals. In the cervical lymph nodes of the *Tag+/+* EAE-induced mice these cells were found to be reduced when compared to those of *Tag1-/-* EAE-induced mice (data not shown). However in this case the result is less reliable as the number of cells that were analyzed, highly differed between the two genotypes.

The finding that T_{reg} cells, responsible for the development of self-tolerance, are significantly reduced in the spinal cord and at the same time are increased in the lymph nodes of *Tag1-/-* EAE-induced mice around the peak of the symptoms, might point to an abnormality in mechanisms governing autoimmunity.

D. Discussion

D.1. Molecular analysis of the TAG-1/Caspr2 interaction

D.1.1. Characterization of the TAG-1 subdomains implicated in its interaction with Caspr2

The efficient propagation of the axon potentials along myelinating axons is of high importance for many motor, sensory and cognitive functions of vertebrates. This process requires the precise distribution of ion channels at the nodes of Ranvier. TAG-1 and Caspr2 are CAMs required for the clustering of VGKCs Kv1.1/Kv1.2 at the juxtaparanodes of myelinated axons. These channels are especially crucial for stabilizing conduction during myelination of the developing axons that switch from a continuous to a saltatory mode of conduction (Vabnick et al., 1999). Such a function of VGKCs may also operate in demyelination-remyelination events in MS. MS pathology has been associated with alterations of the nodes of Ranvier including diffusion of the juxtaparanodal Kv1 channels.

The absence of either TAG-1 or Caspr2 results in a disruption of the juxtaparanodal complex and subsequent diffusion of the VGKCs towards the internodes. The role of the TAG-1/Caspr2 complex is possibly the maintenance of the VGKCs at the juxtaparanodal region (Poliak et al., 2003; Traka et al., 2003; Savvaki et al., 2008; Traka et al., 2002; Horresh et al 2008).

TAG-1interacts in an homophilic way with itself *In trans*, through its FNIII-repeats (Tsiotra et al., 1996). On the contrary, axonal TAG-1 interacts in a heterophilic way, *in cis* with Caspr2 and VGKCs through its Ig-like modules (Tzimourakas et al., 2007). Moreover, glial TAG-1 can physically interact with Caspr2 (*in trans*) and is sufficient for the formation of the Juxtaparanodal complex (Savvaki et al., 2010).

Furthermore, it is worth mentioning that autoantibodies against both TAG-1 and Caspr2 have been identified in MS patients and in VGKC autoimmune diseases respectively (Derfuss et al., 2009; Irani et al., 2010; Lancaster et al., 2011).

We are convinced that further understanding the molecular and functional interactions between CAMs and ion channels may lead to important insights into the pathogenesis of MS. Additionally, knowledge of these mechanisms is expected to contribute to the development of clinical strategies towards the functioncal restoration of axonal disorganization/degeneration in demyelinating diseases such as MS.

In the first part of this study we tried to identify the specific regions that are implicated in the interaction between the CAMs TAG-1 and Caspr2. After confirming the previous observations that the total TAG-1 molecule and the Ig1-6 subdomains of TAG-1(alone) interact with Caspr2, we came up to some unexpected observations. Firstly, the FNIII (1-4) subdomains of TAG-1 could also interact with Caspr2, something that is contradictory with what was observed in the publication of Tzimourakas et al., 2007. Furthermore, even though the Ig1-4, Ig1-2 and Ig3-4 subdomains of TAG-1 could interact with Caspr2, an Ig1-5 subdomain of TAG-1 and Caspr2 interaction could not be detected. This is opposite from what we would expect as all these subdomains (Ig1-4, Ig1-2 and Ig3-4) are smaller parts

included in the Ig1-5 subdomain. Last but not least, the Ig5-6 + FN1-2 subdomain of TAG-1, was also able to interact with Caspr2.

The reason why in the Tzimourakas et al., 2007 an interaction between the Ig1-6 subdomains was detected, while the interaction of FN1-4 subdomains was not observed is not known. A possible explanation is that in the plasmid constructs that were used in this study, the signal peptide sequence was inserted at the C-terminal of GFP. As a result, the expression of GFP would not be chimeric with the FN1-4 subdomains, due to removal of the signal peptide during a sorting process that usually takes place when a transmembrane protein is directed to Endoplasmic Reticulum (ER). The signal sequences are often found at the N-terminal of proteins and signal peptidases remove them from the "mature" protein once the sorting process is complete (Alberts et al, 2008). Thus, as an α-GFP antibody was used in order to detect the FN1-4 subdomains of TAG-1 both in the co-IP and the WB experiments, it would not have been possible to detect the existing interaction of these subdomains and Caspr2. This problem did not affect the identification of the Ig1-6 and Caspr2 interaction as in this case an α-TAG-1 antibody was used.

The observation that the only subdomain of TAG-1 which was not found to interact with Caspr2 was the Ig1-5 is mysterious. The simplest explanation that we could give is a possible important alteration in the 3D conformation of the polypeptide produced in this case. This alteration could result in the concealment of all potent interaction sites of the two molecules, which does not take place in any other case. It was shown for example in Freigang et al. 2000 that there is a contact between Ig domains 1 and 4 and domains 2 and 3 in the Ig1-4 subdomains alone. The situation could differ in different combinations of the TAG-1 subdomains. However, this is just a hypothesis which would need further investigation. At this point, it is worth mentioning that our collaborators from the laboratory of Dr Faivre-Sarrailh (Aix Marseille University) could detect interaction of TAG-1 with all four deletion mutants of Caspr2 they used, in similar experiments.

Furthermore, two recent studies present contradictory results concerning the interaction of Capsr2 and TAG-1. More specifically, in the first study (Rubio-Marrero et al., 2016) even though a direct interaction of Caspr2 and Contactin-1 with high μM affinity was detected - through biophysical techniques and bio-layer interferometry (BLI)- under the same conditions this was not observed for Contactin-2 and Caspr2. The authors when trying to explain why the latter interaction was not detected in their experiments (even though it has been previously reported multiple times), propose that this is due to the fact that the affinity of the Caspr2/TAG-1 pair is currently unknown and maybe this interaction is significantly weaker than the interaction of Contactin-1 and Caspr2. An even more recent study (Lu et al., 2016) confirmed the interaction between TAG-1 and Caspr2 with high affinity and low nanomolar range, through surface Plasmon resonance (SPR). Moreover in this publication it was shown that the extracellular domains of Caspr2 and TAG-1 bind each other tightly and specifically. These two studies focused on the structural characterization of Caspr2 and revealed many differences. Nevertheless, the fact that the ability of Caspr2 to recruit partners is heavily influenced by how the molecules (including Caspr2 itself) are positioned in the extracellular space, is highlighted in both studies. Caspr2 is a membrane protein and in

both studies it was purified and used in a soluble form, which may be significantly different than the natural form.

Collectively, the conformation of CAMs and their subdomains seem to play an important role in their affinity and interaction and it would be important to further investigate the structure of the TAG-1/Caspr2 complex. Concerning this, we are planning to produce some more TAG-1 deletion constructs (e.g. Ig1-3 and Ig4-5) in order to get more insight on the subdomains of TAG-1 that are capable to interact with Caspr2. Furthermore, othe Ig-CAMs that are known not to interact with TAG-1 can be used as controls. However, more complicated methods such as cross-linking/mass spectrometry and crystallography could probably give more trustworthy results on what exactly the situation is. The fact that the entire human TAG-1 protein has not been crystallized makes it difficult to extrapolate information for the 3D structure of its subdomains.

D.1.2. The effect of a released form of TAG-1 in its interaction with Caspr2

Previous experiments in our lab (Savvaki et al., 2010) had shown that the protein TAG-1 is released from oligodendrocyte cultures that express it transgenically. In the transgenic mice "Tag-$1^{-/-}$;$plp^{tg(rTag-1)}$" TAG-1 was expressed exclusively from oligodendrocytes, while Caspr2 was normally localized at the juxtaparanodal region of the myelinated fibers. In these transgenic mice it was shown that glial TAG-1 interacts with Caspr2 (*in trans*), at the juxtaparanodes, in the absence of axonal TAG-1. In the experiments where the interaction was detected, the transgenic protein was observed, except for the surface of the oligodendrocytes, in a released form at the supernatant as well. In this publication, for the first time the *trans* interaction of glial TAG-1 and Caspr2 is mentioned, without excluding the possibility that the secreted form of TAG-1 might play a role in this interaction and thus in the formation of the juxtaparanodal complex. These observations, may suggest the presence of a released form of TAG-1 as a "collaborator" to the GPI-anchored glial TAG-1 (figure 30). This collaborator could be either the secreted form of TAG-1 or a yet unidentified molecule.

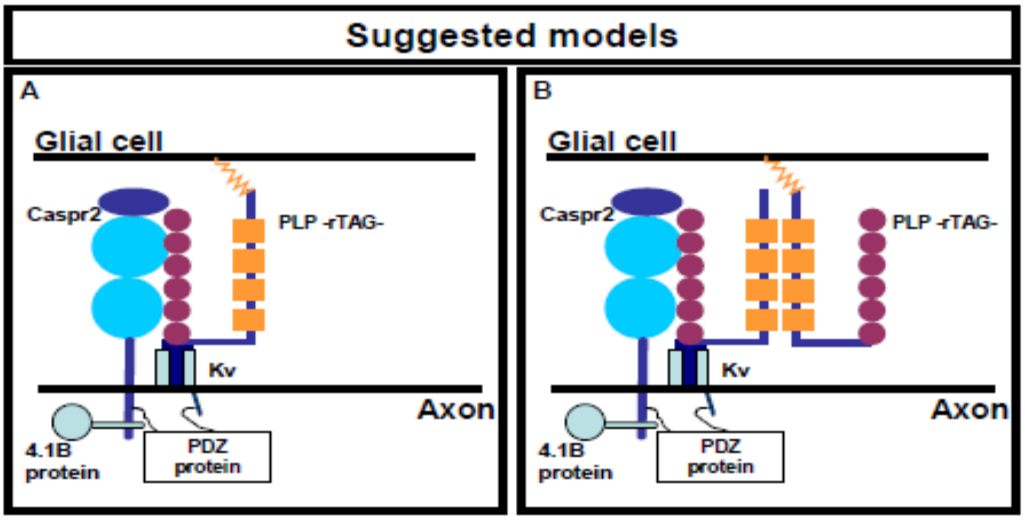

Figure 30: Proposed models of the axo-glial interactions between the proteins of the juxtaparanodal region in the CNS. A) In the absence of axonal TAG-1, glial TAG-1 interacts with Caspr2 and Kv channels which are placed on the axon. B) The GPI-anchored glial TAG-1, interacts and

forms a homodimer with the released form of TAG-1 which in turn interact with other proteins of the juxtaparanodal region (Savvaki Maria, 2010-PhD thesis).

In the case of the wild type, the *trans* homophilic interaction of TAG-1 might be the first step towards the formation of the juxtaparanodal complex, which is followed by the *cis* interaction of TAG-1 with Caspr2. In the Savvaki et al., 2010 publication it is also suggested that the *cis* interaction of TAG-1 with Caspr2 on the axon, might not be required for the formation of the complex. A possible role of axonal TAG-1 could be the stabilization of the axo-glial interaction between the axonal Caspr2 and the TAG-1 molecule that is expressed from oligodendrocytes. It is moreover mentioned a possibility that the role of TAG-1 in the case of the transgenic situation, could be replaced by the released form of TAG-1. Thus we tried to examine whether the released/secreted form of TAG-1, mediates somehow the *cis* interaction of the GPI-anchored TAG-1 with Caspr2.

Our results did not show any visible effect on the interaction of total TAG-1 with Caspr2. However, when the Ig1-6/Caspr2 and Fn1-4/Caspr2 interactions were checked after the addition of secreted TAG-1, the signal of the co-precipitated Caspr2 seemed less intense. However, this is just an optical observation and since co-IP is a non-quantitative technique we cannot make “safe” conclusions.

D.2. Sema6A and Neurofascin isoforms 140 and 150 are novel interactors of TAG-1

In this part of the study, we took advantage of the user-friendly computational tool UniReD (Dr Iliopoulos Ioannis lab), which can not only identify all known interactors of a molecule, but it can predict novel interactors based on known Biomedical literature stored in various biomedical related databases. Here we used this tool in order to identify potent interactors of the target molecule TAG-1. Two molecules that were predicted to interact with TAG-1 were Sema6A and Neurofascin which we confirmed experimentally. The validation took place after co-transfection in HEK293 cells and co-Immunoprecipiation experiments, as an interaction was detected between TAG-1 and Sema6A, Neurofascin 140 and 155. The verification through these experiments suggests that the reliability of this computational tool is of high significance, especially when taking into consideration that also other potent interactors have been validated both in our lab and other labs as well (unpublished data).

Sema6A is a class of Semaphorins (Semas) and is a transmembrane guidance molecule involved in thalamocortical (Little et al., 2009) and corticospinal tract (Runker et al.,2008) pathfinding as well as hippocampal (Suto et al., 2007) and cerebellar granule cell migration (Renaud et al., 2008). Moreover, Sema6A is expressed on postnatal oligodendrocytes and has been linked to differentiation and myelinating capacities (Bernard et al., 2012) Furthermore, Sema6A is inhibitory to TAG-1 expressing sensory axons entering the spinal cord from the dorsal roots and is a key regulator of sensory axon growth through the spinal cord during development (Barry et al., 2015).

Neurofascins are known to mediate axo-glial interactions and are essential for the assembly of the nodal complex. The Neurofascin gene encodes a glial isoform NF155 which is found

mainly at the paranode and a neuronal isofrom NF186 found mainly at the nodes. However both of them have key roles in the clustering of sodium channels (Sherman et al., 2005). More recently a third isoform NF140, was found to be an embryonic neuronal neurofascin that promotes the assembly of the Nodes of Ranvier. Interestingly, NF140 is reexpressed in demyelinating MS lesions (Zhang et al., 2015).

Autoantibodies have been detected against both Neurofascin and TAG-1 in MS patients and may also induce gray matter alterations (Derfuss et al., 2009; Mathey et al., 2007).

Taken together, we strongly believe that UniReD is a very rapid, helpful and innovative tool towards the identification of novel proteins that interact with the protein of interest that can also extract known interactions accurately. The verified novel interactors of TAG-1 could be of high importance and further investigation needs to be followed in order to examine in which developmental and/or pathological stages the interactions take place in vivo and which are the roles that they serve.

D.3. Study of EAE in wild type versus *Tag-1-/-* mice

The EAE mouse model is one of the most commonly used demyelination models and EAE studies have greatly contributed to the understanding of basic MS pathology. It has been shown that the histopathology of EAE mimics that of MS in several aspects, such as that it is a T-cell-driven disease and that these cells are autoreactive against myelin components (i.e. MBP, MOG and PLP). Furthermore in both cases WM lesions fail to remyelinate and axonal loss can be observed (Waksman and Adams 1962, Yasuda, et al. 1975, Bernard, et al. 1976, Steinman and Zamvil 2006, Croxford, et al. 2011). However some striking differences occur between EAE and MS. For example, in the C57BL/6 mouse strain, the disease is induced by a harsh induction and is monophasic, while MS is spontaneous and dynamic. Additionally, in EAE, lesions are found only in the spinal cord WM and are mostly dominated by CD4+ T-cells, while MS plaques are found also in the brain, both in WM and GM and the disease is mostly CD8+ T-cell-driven. Last but not least, a limitation of EAE is that it is not permissive for remyelination studies, since even at chronic stages the inflammatory environment is such that remyelination is only partial (Paterson and Day 1979).

As mentioned, *Tag1-/-* mice exhibit significant hypomyelination of the optic nerve, apart from the juxtaparanodal alterations already discussed (Chatzopoulou et al., 2008). Our goal was to subject wild type and knock-out mice to EAE and compare their clinical, histopathological and immunological findings during the acute and chronic phase of the induced disease.

Mice lacking TAG-1 are characterized by the same onset as wild type animals, but show a delay of 3-5 days to reach the peak of the symptoms. However, in both cases remission was observed 2-4 days after the peak. The recovery lasted longer in wild type mice and interestingly, the symptom severity was significantly higher at *Tag-1-/-* mice during the RR stage of the disease both compared to *Tag-1+/+* at the same time point and compared to the first relapse episode of the knock-out mice.

The progression of neurological decline in EAE has been associated with increase in mononuclear cell numbers in the spinal cord and selective loss of small caliber axons of the corticospinal tract, since the observed axonal loss, synchronous with disease onset, is not further increased with disease progression (Black et al., 2006; Soulika et al., 2009). In *Tag-1-/-* mice, ultrastractural Electron Microscopy (EM) analysis has shown a reduction in small caliber axons of the optic nerve and an increase in large caliber axons (Chatzopoulou et al., 2008; Savvaki et al., 2010). Although no such analysis has been performed on axons of the spinal cord, we could hypothesize that the loss of small caliber axons could occur in the spinal cord as well, since the juxtaparanodal phenotype is similar in both tissues. The decreased progression of symptoms in knock-out mice might be due to decreased rate of axonal degeneration in the spinal cord, taking into account that small caliber axons are more susceptible to axonopathy and larger caliber axons would develop the pathology slower.

Concerning demyelination, a few days after the peak of the disease (20dpi) the entire length of the spinal cord seemed to be affected in the case of wild type mice. On the other hand, in mice lacking TAG-1, mostly lumbar areas were vulnerable to demyelination. At 40dpi only the cervical and thoracic areas were analyzed, and were found to present similar demyelination degree. Additionally, in wild type mice at 20dpi the degree of demyelination correlated the axonal loss severity. In the cervical spinal cord of knock-out mice however, axonal loss was detected in higher degree when correlated with the demyelinated area, something that was also observed at chronic EAE (40dpi). Collectively, the knock-out mice seem more vulnerable to axonal loss, as in the wild type animals it has been reduced at 40dpi while in the knock-out mice it remains at the same levels mostly in the cervical area.

EAE is considered a model which resembles mainly the immunological aspects of MS, as it presents high inflammation due to an immune system attack. Thus, a great deal of characterization of all immunological processes and involved cell types has been made. MS is considered a CD8+ T-cell driven disease, while lesions are also populated by smaller numbers of CD4+ T cells (Huseby et al., 2001). Moreover, MS and EAE tissues are characterized by the activation of microglial cells and infiltration by macrophages.

TAG-1 had no effect on total infiltrating numbers of T and B cells in the spinal cord of EAE-induced mice. However, a significant difference was observed in the CD4+;CD25+;Foxp3+ T cell subpopulation, which is also known as regulatory T cells, as it was found notably decreased in knock-out mice at the peak of the symptoms in two separate experiments. Furthermore, T_{regs} were found to be decreased at the lymph nodes of wild type mice when compared to the knock-out animals.

T_{regs} are thought to be a key component of autoimmunity, as under normal circumastances, naturally arising T_{regs} in the thymus are responsible for the development of self-tolerance and homeostasis at the periphery (Sagakuchi, 2004). Additionally, T_{regs} are thought to exert the suppression of autoimmunity through interaction with antigen-presenting cells (APCs) in a variety of proposed mechanisms.

As already analyzed, apart from its localization at the juxtaparanodes, TAG-1 is implicated in various processes such as neurogenesis, neurite outgrowth, fasciculation etc. (Karagogeos, 2003). Although the expression and role of the protein has been extensively described in the

nervous system, its expression in the immune system was firstly documented only recently (Alvarez et al., 2015), where TAG-1 was found to be a tissue-restricted antigen (TRA), normally expressed by thymic epithelial cells. The expression of any TRA by these cells ensures the development of tolerance of the immune system against this protein. Our findings point to a potential direct implication of the protein in driving autoimmune responses, opposed to the idea that it was only an autoantigen (Derfuss et al., 2009). TAG-1 could be expressed by a cell population of the immune system acting directly or indirectly on T_{regs} or it might even be present in the latter cell type.

Taking into consideration the proposed role of TAG-1 as a key in the shaping of shelf tolerance, we could hypothesize that its absence during thymic clonal selection might have an effect on the establishment of the population of T_{regs}. Further investigation of the cells of the immune system should be done, not only in induced animals, but also in naïve knock-out mice in order to uncover any potential involvement of the protein in either normal or pathology-driven responses of the immune system. Finally, since the human immune system differs in many ways from that of mice, it would be interesting to analyze the expression of TAG-1 in the human immune system as well.

E. References

1) Nave, K. A. and Werner, H.B. (2014) "Myelination of the Nervous System: Mechanisms and Functions." *Annu. Rev. Cell Dev. Biol.* **30**: 503-33
2) Arroyo, E. J. and S. S. Scherer (2000). "On the molecular architecture of myelinated fibers." *Histochem Cell Biol* **113**(1): 1-18.
3) Saher, G., Brugger, B., Lappe-Siefke, C., Mobius, W., Tozawa, R., Wehr, M.C., Wieland, F., Ishibashi, S. and Nave K.A. (2005) "High cholesterol level is essential for myelin membrane growth." *Nat Neurosci* **8**(4):468-475
4) Poliak, S. and E. Peles (2003). "The local differentiation of myelinated axons at nodes of Ranvier." Nat Rev Neurosci **4**(12): 968-980
5) Zoupi, L., Savvaki, M. and Karagogeos, D. (2011)" Axons and myelinating glia: an intimate contact." *IUBMB Life* **63(9)**, 730-735
6) Karagogeos, D. (2003) "Neural GPI-anchored cell adhesion molecules." *Front Biosci.* **8**, s1304-s1320
7) Pan, Z., Kao, T., Horvath, Z., Lemos, J., Sul, J. Y., Cranstoun, S. D., Bennett, V., Scherer, S.S. and Cooper, E. C. (2006). "A common ankyrin-G-based mechanism retains KCNQ and Na_v channels at electrically active domains of the axon." *J Neurosci* **26**(10): 2599-2613
8) Boiko, T., Rasband, M. N., Levinson, S. R., Caldwell, J. H., Mandel, G., Trimmer, J. S. and Matthews G. (2001). "Compact myelin dictates the differential targeting of two sodium channel isoforms in the same axon." *Neuron* **30**(1): 91-104
9) Kaplan, M. R., Cho, M. H., Ullian, E. M., Isom, L. L., Levinson, S. R., and Barres, B. A. (2001). "Differential control of clustering of the sodium channels Na(v)1.2 and Na(v)1.6 at developing CNS nodes of Ranvier." *Neuron* **30**(1): 105-119.
10) Feinberg, K., Y. Eshed-Eisenbach, S. Frechter, V. Amor, D. Salomon, H. Sabanay, J. L. Dupree, M. Grumet, P. J. Brophy, P. Shrager and E. Peles (2010). "A glial signal consisting of gliomedin and NrCAM clusters axonal Na+ channels during the formation of nodes of Ranvier." *Neuron* **65**(4): 490-502.
11) Poliak, S., Gollan, L., Martinez, R., Custer, A., Einheber, S., Salzer, J. L., Trimmer. J. S., Shrager, P. and Peles, E. (1999) Caspr2, a new member of the neurexin superfamily, is localized at the juxtaparanodes of myelinated axons and associates with K+ channels. *Neuron* **24**, 1031-1047
12) Traka, M., Dupree, J. L., Popko, B. and Karagogeos D. (2002) The neuronal adhesion protein TAG-1 is expressed by Schwann cells and oligodentdrocytes and is localized ti the juxtaparanodal region of myelinated fibers. *Journal of Neuroscience* **22**, 3016-24
13) Bhat, M. A., Rios, J. C., Lu, Y., Garcia-Fresco, G.P., Ching, W., St Martin, M., Li, J., Einheber, S., Chesier, M., Rosenbluth, J., Saizer, J.L. and Bellen, H.J. (2001) "Axon-glia interactions and the domain organization of myelinated axons requires neurexin IV/Caspr/Paranodin." *Neuron* **30**(2): 369-383
14) Boyle, M. E., Berglund, E. O., Murai, K.K., Weber, L., Peles, E, and Ranscht, B. (2001) "Contactin orchestrates assembly of the septate-like junctions at the paranode in myelinated peripheral nerve." *Neuron* **30**(2): 385-397
15) Charles, P., Tait, S., Faivre-Sarrailh, C., Gunn-Moore, F., Denisenko-Nehrbass, N., Guennoc, A.M., Brophy, P.J. and Lubetzki, C. (2002) "Neurofascin is a glial receptor

for the paranodin/Caspr-contactin axonal complex at the aco-glial junction" *Curr Biol* **12**(3):217-20.

16) Girault, J.A. and Peles, E. (2002) "Development of nodes of Ranvier" *Curr Opin Neurobiol* **12**(5):1476-85
17) Susuki, K. and Rasband, M.N. (2008) "Molecular mechanisms of node of Ranvier formation" *Curr Opin Cell Biol* **20**(6):616-23
18) Karagogeos, D., Morton, S.B., Casano, F., Dodd, J., and Jessell, T. M. (1991) "Developmental expression of the axonal glycoprotein TAG-1: differential regulation by central and peripheral neurons *in vitro." Development*. **112**(1), 51-67
19) Poliak, S., Salomon, D., Elhanany, H., Sabanay, H., Kiernan, B., Pevny, L., Stewart, C. L., Xu,X., Chiu, S., Shrager, P., Furley, A. J. W. and Peles, E. (2003) "Juxtaparanodal clustering of *Shaker*-like K+ channels in myelinated axons depends on Caspr2 and TAG-1." *The journal of Cell Biology* **162**, 1149-1160
20) Traka, M., Goutebroze, L., Denisenko, N., Bessa, M., Nifli, A., Havaki, S., Iwakura, Y., Fukamauchi, F., Watanabe, K., Soliven, B., Girault, J. A., Karagogeos D. (2003) "Association of TAG-1 with Caspr2 is essential for the molecular organization of juxtaparanodal regions of myelinated fibers." *J. Cell Biology* **162,** 1161-1172
21) Savvaki, M., Panagiotaropoulos, T., Stamatakis, A., Sargiannidou, I., Karatzioula, P., Watanabe, K., Stylianopoulou, F., Karagogeos, D. and Kleopa, K. A. (2008) "Impairment of learning and memory in TAG-1 deficient mice associated with shorter CNS internodes and disrupted juxtaparanodes." *Molecular and Cellular Neuroscience* **39**, 478-490
22) Denisenko-Nehrbass, N., Oquievetskaia, K., Goutebroze, L., Galvez, T., Yamakawa, H., Ohara, O., Carnaud, M. and Girault, J. A. (2003) "Protein 4.1B associates with both Caspr/paranodin and Caspr2 at paranodes and juxtaparanodes of myelinated fibers." *The European Journal of Neuroscience* **17***(2),* 411-6
23) Horresh, I., Poliak, S., Grant, S., Bredt, D., Rasband, M. N. and Peles, E. (2008) "Multiple molecular interactions determine the clustering of Caspr2 and Kv1 channels in myelinated axons." *The Journal of Neuroscience* **28**, 14213-14222
24) Ogawa, Y., and Rasband, M. N. (2009) "Proteomic analysis of optic nerve lipid rafts reveals new paranodal proteins." *The Journal of Neuroscience* Res.**87**, 3502-3510
25) Spiegel, I. and E. Peles (2002) "Cellular junctions of myelinated nerves (Review)." *Mol Membr Biol* **19**(2): 95-101
26) Hynes, R. O. and Zhao, Q. (2000) "The evolution of cell adhesion." J *Cell Biol* **150**(2): F89-96.
27) Williams, A. F. and Barclay, A. N. (1988) "The immunoglobulin superfamily domains for cell surface recognition." *Annu Rev Immunol* **6**: 381-405.
28) Zhang, A., Desmazieres, A., Zonta, B.,Melrose, S., Campbell, G., Mahad, D., Li, Q., Sherman, D.L., Reynolds, R. and Brophy, P.J. (2015) "Neurofascin 140 is an embryonic neuronal neurofascin isoform that prootes the assembly of the node of Ranvier" *j. Neurosci* **35**(5):2246-54
29) Sherman, D.L., Trait, S., Melrose, S., Johnson, R., Zonta, B., Court, F.A., Macklin, W.B., Meek, S., Smith, A.J., Cottrell, D.F. and Brophy, P.J. (2005) "Neurofascins are required to establish axonal domains for salutatory conduction" *Neuron* **45**(5):737-42

30) Tsiotra, P. C., Theodorakis, K., Papamatheakis, J. and Karagogeos, D. (1996) “The fibronectin domains of the neural adhesion molecule TAX-1 are necessary and sufficient for hemophilic Binding.” *The journal of Biological Chemistry* **271**, 29216-29222
31) Tzimourakas, A., Giasemi, S., Mouratidou, M. and Karagogeos, D. (2007) “Structure-function of protein complexes involved in the molecular architecture of juxtaparanodal regions of myelinated fibers.” *Biotechnology Journal* **2**, 577-83
32) Savvaki, M., Theodorakis, K., Zoupi, L., Stamatakis, A., Tivodar, S., Kyriacou, K., Stylianopoulou, F. and Karagogeos, D. (2010) “The expression of TAG-1 in glial cells is sufficient for the formation of the juxtaparanodal complex and the phenotypic rescue of Tag-1 Homozygous mutants in the CNS.” *The Journal of Neuroscience* **30**, 13943-13954
33) Pavlou, O., Theodorakis, K., Falk, J., Kutsche, M., Schachner, M., Faivre-Sarrailh, C. and Karagogeos, D. (2002) “Analysis of interactions of the adhesion molecule TAG-1 and its domains with other Immunoglobulin Superfamily members.” *Molecular and cellular Neuroscience* **20**, 367-381
34) Freigang, J., Proba, K., Leder, L., Diederichs, K., Sonderegger, P. and Welte, W. (2000) “The crystal structure of the ligand bindin module of axonin-1/TAG-1 suggests a zipper mechanism for neural cell adhesion.” *Cell* **101**: 425-433
35) Tsiotra, P. C., Karagogeos, D., Theodorakis, K., Michaelidis, T. M., Modi, W. S., Furley, A. J., Jessell, T. M. and Papamatheakis, J. (1993) “Isolation of the cDNA and chromosomal localization of the gene (TAX1) encoding the human axonal glycoprotein TAG-1.” *Genomics* **18**, 562-567
36) Denaxa, M., Pavlou, O., Tsiotra, P., Papadopoulos G. C., Liapaki, K., Theodorakis, K., Papadaki, C., Karagogeos, D. and Papamatheakis, J. (2003) “The upstream regulatory region of the gene for the human homologue of the adhesion molecule TAG-1 contains elements driving neural specific expression in vivo.” *Molecular Brain Research* **118**, 91-101
37) Wolfer, D. P., Giger, R. J., Stagliar, M., Sonderegger, P. and Lipp, H.P. (1998) “Expression of the axon growth-related neural adhesion molecule TAG-1/axonin-1 in the adult mouse brain.” *Anat Embryol (Berl)* **197**(3): 177-185.
38) Yoshihara, Y., Kawasaki, M., Tamada, A., Nagata, S., Kagamiyama, H. and Mori, K. (1995) “Overlapping and differential expression of BIG-2, BIG-1, TAG-1, and F3: four members of an axon-associated cell adhesion molecule subgroup of the immunoglobulin superfamily.” *J Neurobiol* **28**(1): 51-69
39) Denaxa, M., Chan, C. H., Schancher, M., Parnavelas, J.G. and Karagogeos, D.(2001) “The adhesion molecule TAG-1 mediates the migration of cortical interneurons from the ganglionic eminence along the corticofugal fiber system.” *Development* **128**(22): 4635-4644
40) Chatzopoulou, E.,. Miguez, A. Savvaki, M., Levasseur, G., Muzerelle,A., Muriel, M. P., Goureau, O., Watanabe, K., Goutebroze, L., Gaspar, P., Zalc, P., Karagogeos D. and Thomas J. L. (2008). “Structural requirement of TAG-1 for retinal ganglion cell axons and myelin in the mouse optic nerve.” *J Neurosci* **28**(30): 7624-7636.
41) Derfuss, T., Parikh, K., Velhin, S., Braun, M., Mathey, E., Krumbholz, M., Kumpfel, T., Moldenhauer, A., Rader, C., Sonderegger, P., Pollmann, W., Tiefenthaller, C., Bauer,

J., Lassmann, Hans. L., Wekerle, H., Karagogeos, D., Hohlfeld, R., Linington, C. and Meinl, E. (2009). “Contactin-2/TAG-1-directed autoimmunity is identified in multiple sclerosis patients and mediates gray matter pathology in animals.” *PNAS* **106:** 8302-8307

42) Alvarez, I., Collado, J. A., Colobran R., Carrascal, M., Ciudad, M. T., Canals, F., James, E. A., Kwok, W. W., Gartner, M., Kyewski, B., Pujol-Borrell, R. and Jaraquemada D. (2015) “Central T cell tolerance: Identification of tissue-restricted autoantigens in the thymus HLA-DR peptidome.” *J Autoimmun* **60**: 12-19.
43) Lassmann, H. (1998) “Neuropathology in multiple sclerosis: new concepts.” *Mult Scler* **4**(3): 93-98
44) Ruzman, R., Chen, X. and Li, Y.M. (2012) “Gray matter involvement in patients with multiple sclerosis by magnetic resonance imaging.” *Chin Med J (Engl)* **125**(13):2361-4
45) Barnett, M.H., Henderson, A.P. and Prineas, J.W. (2006) “The machrophage in MS: just a scavenger after all? Pathology and pathogenesis of the acute MS lesion.” *Mult Scler* **12**(2):121-32
46) Handerson, A.P., Barnett, M.H., Parratt, J.D. and Prineas, J.W. (2009) Multiple sclerosis: distribution of inflammatory cells in newly forming lesions.” *Ann Neurol **66*** (6): 739-53
47) Nikic, I., D. Merkler, C. Sorbara, M. Brinkoetter, M. Kreutzfeldt, F. M. Bareyre, W. Bruck, D. Bishop, T. Misgeld and M. Kerschensteiner (2011). “A reversible form of axon damage in experimental autoimmune encephalomyelitis and multiple sclerosis.” *Nat Med* **17**(4): 495-499.
48) Rudick, R.A. and Trapp, B.D. (2009) “Gray-matter injury in multiple sclerosis.” *N Engl J Med* **361**(15):1505-6
49) Stassart, R.M., Fledrich, R., Velanac, V., Brinkmann, B.G., Schwab, M.H., Meijer, D., Sereda, M.W. and Nave, K.A. (2013) “A role for Schwann cell-derived neuregulin-1 in remyelination” *Nat Neurosci* **16**(1):6122-31
50) Franklin, R. J. and Ffrench-Constant, C. (2008) “Remyelination in the CNS: from biology to therapy.” *Nat Rev Neurosci* **9**(11): 839-855.
51) Lindberg, R.L.P. and Kappos, L., (2006) “ Transcriptional profiling of multiple sclerosis: towards improved diagnosis and treatment” *Expert Rev Mol Diagn* **6**(6): 843-55
52) Tisell, A., Leinhard, O.D., Warntjes, J.B., Aalto, A., Smedby, O., Landtblom, A.M. and Lundberg, P. (2013) “Increased concentrations of glutamate and glutamine in normal-appearing white matter of patients with multiple sclerosis and normal MR imaging brain scans.” *PLoS One* 8(4):e61817
53) Serafini, B., Rosicarelli, B. Magliozzi, R., Stigliano, E. and Aloisi, F. (2004) "Detection of ectopic B-cell follicles with germinal centers in the meninges of patients with secondary progressive multiple sclerosis." *Brain Pathol* **14**(2): 164-174.
54) Steinman, L. and Zamvil, S. (2003). “Transcriptional analysis of targets in multiple sclerosis.” *Nature Rev Immunol* **3**(6): 483-92
55) George, M. F., Briggs, F.B., Shao, X., Gianfrancesco, M. A., Kockum, I Harbo, H. F., Celius, E. G., Bos, S. D.,Hedstrom, A., Shen, L., Bernstein, A., Alfredsson, L., Hillert, J., Olsson, T., Patsopoulos, N. A., De Jager, P. L., Oturai, A. B., Sondergaard, H.B., Sellebjerg, F., Sorenser, P. S., Gomez, R., Caillier, S. J., Cree, B. A., Oksenberg, J. R.,

Hauser, S. L., D'Alfonso, S., Leone, M. A., Martinelli Boneschi, F., Soroshina M., van der Mei, I., Taylor, B.V., Zhou, Y., Schaefer, C. and Barcellos, L. F. (2016). "Multiple sclerosis risk loci and disease severity in 7,125 individuals from 10 studies." *Neurol Genet* **2**(4): e87

56) Coman, I., Aigrot, M. S., Seilhean, D., Reynolds, R., Girault, J. A., Zalc, B. and Lubetzki, . (2006) "Nodal, paranodal and juxtaparanodal axonal proteins during demyelination and remyelination in multiple sclerosis." *Brain* **129**(Pt 12): 3186-3195
57) Zoupi, L., Markoullis, K., Kleopa, K. A. and Karagogeos, D. (2013) "Alterations of juxtaparanodal domains in two rodent models of CNS Demyelination." *Glia* **61,** 1236-49
58) Kastriti, M.E., Sargiannidou, I., Kleopa, K.A. and Karagogeos,D. (2015) "Differential modulation of the juxtaparanodal complex in Multiple Sclerosis" *Molecular and Cellular Neuroscience* **67**: 93-103
59) Mathey, E. K., Derfuss, T., Storch, M. K., Williams, K. R., Hales, K., et al (2007) "Neurofascin as a novel target for autoantibody-mediated axonal injury." *J. Exp. Med.* **204**, 2363-2372
60) Ransohoff., R. M. (2012). "Animal models of multiple sclerosis: the good, the bad and the bottom line." *Nat Neurosci* **15**(8): 1074-1077
61) Steinman, L. and Zamvil, S. S. (2006). "How to successfully apply animal studies in experimental allergic encephalomyelitis to research on multiple sclerosis." *Ann Neurol* **60**(1): 12-21.
62) Croxford, A. L., Kurschus, F. C. and. Waisman A. (2011). "Mouse models for multiple sclerosis: historical facts and future implications." *Biochim Biophys Acta* **1812**(2): 177-183.
63) Steinman, L. and Zamvil, S. S. (2006). "How to successfully apply animal studies in experimental allergic encephalomyelitis to research on multiple sclerosis." *Ann Neurol* **60**(1): 12-21.
64) Croxford, A. L., Kurschus, F. C. and. Waisman A. (2011). "Mouse models for multiple sclerosis: historical facts and future implications." *Biochim Biophys Acta* **1812**(2): 177-183.
65) Steinman, L. and Zamvil, S. S. (2006). "How to successfully apply animal studies in experimental allergic encephalomyelitis to research on multiple sclerosis." *Ann Neurol* **60**(1): 12-21.
66) Croxford, A. L., Kurschus, F. C. and. Waisman A. (2011). "Mouse models for multiple sclerosis: historical facts and future implications." *Biochim Biophys Acta* **1812**(2): 177-183.
67) Huseby, E. S., Liggitt, D. Brabb, T. Schnabel, B. Ohlen C. and J. Goverman (2001). "A pathogenic role for myelin-specific CD8(+) T cells in a model for multiple sclerosis." *J Exp Med* **194**(5): 669-676.
68) Yednock, T. A., Cannon, C., Fritz, L. C., Sanchez-Madrid, F., Steinman, L. and Karin, N. (1992) "Prevention of experimental autoimmune encephalomyelitis by antibodies against alpha 4 beta 1 integrin." *Nature* **356**(6364): 63-66
69) Fukamauchi, F., Aihara, O., Wang., Y. J., Akasaka., K. Takeda., Y., Horie., M., Kawano., H., Sudo., K., Asano., M., Watanab, K., and Iwakura, Y. (2001). "TAG-1-

deficient mice have marked elevation of adenosine A1 receptors in the hippocampus." *Biochem Biophys Res Commun* **281**(1): 220-226.

70) Ioannou, M., T. Alissafi, I. Lazaridis, G. Deraos, J. Matsoukas, A. Gravanis, V. Mastorodemos, A. Plaitakis, A. Sharpe, D. Boumpas and P. Verginis (2012). "Crucial role of granulocytic myeloid-derived suppressor cells in the regulation of central nervous system autoimmune disease." *J Immunol* **188**(3): 1136-1146
71) Schneider, C. A., Rasband W. S., and Eliceiri K. W. (2012). "NIH Image to ImageJ: 25 years of image analysis." *Nat Methods* **9**(7): 671-675.
72) Montgomery, I.N and Rauch, H.C. (1982) "Experimental allergic encephalomyelitis (EAE) in mice: primary control of EAE susceptibility is outside the H-2 complex." *J Immunol* **128**(1):421-5
73) Vabnick, I., Trimmer, J.S., Schwarz, T.L., Levinson, S.R., Risal, D., and Shrager, P. (1999). "Dynamic potassium channel distributions during axonal development prevent aberrant firing patterns." *J Neurosci* **19:** 747-758.
74) Irani, S.R., Alexander, S., Waters, P., Kleopa, K.A., Pettingill, P., Zuliani, L., Peles, E., Buckley, C., Lang, B., and Vincent, A. (2010). "Antibodies to Kv1 potassium channel-complex proteins leucine-rich, glioma inactivated 1 protein and contactin-associated protein-2 in limbic encephalitis, Morvan's syndrome and acquired neuromyotonia." *Brain* **133:** 2734-2748.
75) Lancaster, E., Huijbers, M.G., Bar, V., Boronat, A., Wong, A., Martinez-Hernandez, E., Wilson, C., Jacobs, D., Lai, M., Walker, R.W., Graus, F., Bataller, L., Illa, I., Markx, S., Strauss, K.A., Peles, E., Scherer, S.S., and Dalmau, J. (2011). "Investigations of caspr2, an autoantigen of encephalitis and neuromyotonia." *Ann Neurol* **69:** 303-311
76) Alberts, B., Johnson, A., Lewis, J., Raff, M., Roberts, K. and Walter, P. ;Book: Molecular Biology of the cell, 5th edition (2008) Garland Science
77) Rubio-Marrero, E.N., Vincelli, G., Jeffries, C.M., Shaikh, T.R., Pakos, I.S., Ranaivoson, F.M., von Daake, S., Demeler, B., De Jaco, A., Perkins, G., Ellisman, M.H., Trewhella, J. and Comoletti, D. (2016) "Structural characterization of the extracellular domain of CASPR2 and insights into its association with the novel ligand Contactin1." *J Biol Cehm* **291**(11):5788-802
78) Lu, Z., Reddy, M.V., Liu, J.,Kalichava, A., Liu, J., Zhang, L., Chen, F, Wang, Y., Holthauzen, L.M., White, M.A., Seshadrinathan, S., Zhong, X., Ren, G. and Rudenko, G. (2016) "Molecular architecture of contactin-associated protein-like 2 (CNTNAP2) and its Interaction with Contactin 2 (CNTN2)." *J Biol Chem* pii: jbc.M116.748236
79) Little, G.E., Lopez-Bendito, G., Runker, A.E,, Garcia, N., Pinon, M.C., Chedotal, A., Molnar, Z. and Mitchell, K.J. (2009) "Specificity and plasticity of thalamocortical connections in Sema6A mutant mice." *PLoS biology* 7:e98.
80) Runker, A., Little, G., Suto, F., Fujisawa, H. and Mitchell, K. (2008) "Semaphorin-6A controls guidance of corticospinal tract axons at multiple choice points." *Neural Development* **3**:34
81) Suto, F., Tsuboi, M., Kamiya, H., Mizuno, H., Kiyama, Y., Komai, S., Shimizu, M., Sanbo, M., Yagi, T., Hiromi, Y., Chedotal, A., Mitchell, K.J., Manabe, T. and Fujisawa, H. (2007) "Interactions between plexin-A2, plexin-A4, and semaphorin 6A control lamina-restricted projection of hippocampal mossy fibers." *Neuron* **53**:535-547.

82) Renaud, J., Kerjan, G., Sumita, I., Zagar, Y., Georget, V., Kim, D., Fouquet, C., Suda, K., Sanbo, M., Suto, F., Ackerman, S.L., Mitchell, K.J., Fujisawa, H. and Chedotal, A. (2008) "Plexin-A2 and its ligand, Sema6A, control nucleus-centrosome coupling in migrating granule cells." *Nat Neurosci* **11**:440-449
83) Bernard, F., Moreau-Fauvarque, C., Heitz-Marchaland, C., Zagar, Y., Dumas, L., Fouquet, S., Lee, X., Shao, Z., Mi, S. and Chedota,l A. (2012) Role of transmembrane semaphorin Sema6A in oligodendrocyte differentiation and myelination. *Glia* **60**:1590-1604
84) Barry, D., O'Malley, A., Kelly, A., O'Sullivan, R. and Mitchell, K. (2015) "Semaphorin 6A mediates sensory afferent projection into the developing spinal cord" *The FASEB journal vol. 29 no. 1 Supplement LB42*
85) Waksman, B. H. and Adams, R. D. (1962). "A histologic study of the early lesion in experimental allergic encephalomyelitis in the guinea pig and rabbit." *Am J Pathol* **41**: 135-162
86) Yasuda, T., Tsumita, T., Nagai, Y., Mitsuzawa, E. and Ohtani, S. (1975). "Experimental allergic encephalomyelitis (EAE) in mice. I. Induction of EAE with mouse spinal cord homogenate and myelin basic protein." *Jpn J Exp Med* **45**(5): 423-427
87) Bernard, C., Leydon, C., J. and Mackay, I. R. (1976). "T cell necessity in the pathogenesis of experimental autoimmune encephalomyelitis in mice." *Eur J Immunol* **6**(9): 655-660
88) Paterson, P. Y. and Day, E. D. (1979). "Neuroimmunologic disease: experimental and clinical aspects." *Hosp Pract* **14**(7): 49-58
89) Black, J. A., Liu, S., Hains, B. C., Saab, C. Y., and Waxman, S. G. (2006). "Long-term protection of central axons with phenytoin in monophasic and chronic-relapsing EAE." *Brain* **129**(Pt 12): 3196-3208.
90) Soulika, A. M., Lee, E., McCauley, E., Miers, L., Bannerman, P. and Peasure, P. (2009) "Initiation and progression of axonopathy in experimental autoimmune encephalomyelitis." *J Neurosci* **29**(47): 14965-14979.
91) Huseby, E. S., Liggitt, D. Brabb, T., Schnabel, B., Ohlen, C. and Goverman, J. (2001) "A pathogenic role for myelin-specific CD8(+) T cells in a model for multiple sclerosis." *J Exp Med* **194**(5): 669-676
92) Sakaguchi, S. (2004) "Naturally arising CD4+ regulatory t cells for immunologic self-tolerance and negative control of immune responses" *Annu Rev immunol* **22**:531-62